The Pennsylvania State University
The Graduate School

EQUILIBRIUM PHYSICS IN PARTICULATE FLOW

A Thesis in
Aerospace Engineering
by
Alexander Earl Parkhill

Submitted in Partial Fulfillment
of the Requirements
for the Degree of

Master of Science

August 2008

Reviewed and approved* by the following:

Mario F. Trujillo
Research Associate, Applied Research Laboratory
Thesis Advisor

Robert G. Melton
Professor of Aerospace Engineering
Department of Aerospace Engineering

George A. Lesieutre
Professor of Aerospace Engineering
Head of Department of Aerospace Engineering

*Signatures are on file in the Graduate School.

Abstract

Dynamic equilibrium for particles in one-way momentum coupled flow is studied. The basis for evaluating the particle velocity is a Stokes drag law with gravity that represents a simplified variant of the equation of motion for a rigid sphere (Maxey and Riley 1983). The equilibrium condition, whereby the sum of the forces on the particle is zero, provides an opportunity to reduce computational cost in simulating large numbers of particles. It is shown that the primary parameter that governs deviation from equilibrium is the product of the particle time constant and the maximum eigenvalue of the velocity gradient tensor. This parameter is proposed as a redefinition of the Stokes number for particulate flow. The new Stokes number's effectiveness in predicting departures from equilibrium is demonstrated mathematically and numerically. The analytical conclusions derived from studying the behavior of a particle under a local flow field are supported by simulations in a variety of analytical flow fields. The Lagrangian analysis presented here stands in contrast to many Eulerian formulations presented in the literature, and several limitations involved in using Eulerian techniques are revealed. The Lagrangian solutions presented clarify the physical mechanisms for a particle entering and exiting equilibrium. These solutions are also intended to be used in nonequilibrium situations, avoiding the stiff computational problem of standard particle evolution.

Keywords: Two-phase flow, Lagrangian tracking, particle, droplet, Stokes drag, equilibrium, tracer

Table of Contents

List of Figures

List of Tables

List of Symbols

Subscripts/Superscripts	
$[\cdot]_s$	General Sphere Quantity
$[\cdot]_p$	Particle Quantity
$[\cdot]_f$	Background Fluid Quantity
$[U]_{x,t,xx}$	Partial Derivatives of Background Flow
$[U]^o$	Represents $U(X_s(t=0),0)$

boldface	Vector
typeface	Scalar
$\boldsymbol{V}$	Sphere Velocity
$\boldsymbol{x}$	Sphere Position
$\boldsymbol{U}$	Background Fluid Velocity
$\boldsymbol{g}$	Gravity Force
τ	Time Constant
r	Radius
L_f	Representative Length Scale of the Undisturbed Flow
μ	Dynamic Viscosity
ν	Kinematic Viscosity
$m_{s/p}$	Mass of Sphere/Particle
m_f	Mass of a Sphere Volume of Background Fluid
t	Time
t^*, t'	Dummy Time Integration Variables
$d/dt = \partial/\partial t + \boldsymbol{v} \cdot \nabla$	Lagrangian derivative following the sphere
$D/Dt = \partial/\partial t + \boldsymbol{u} \cdot \nabla$	Lagrangian derivative following a local fluid element

Acknowledgments

I am deeply appreciative of the time, knowledge, and ideas imparted to me by Mario Trujillo. He made my best better throughout my education, and his support was instrumental in completing this thesis. Brian Edge assisted in helping me develop proper coding practices and a proper coding backbone. The majority of this work was supported by funding from the Penn State Applied Research Laboratory Undergraduate Honors Program and is gratefully acknowledged. I would also like to thank the Schreyer Honors College and the College of Engineering for subsidizing my travels.

I am indebted to my friends for many nights out and I look forward to fulfilling these social obligations. To my family I owe the greatest thanks. Somewhere in my upbringing I was taught to grow and enjoy the fruits of education. Thanks to my Mom, my brother Zac, and also to my father, who saw bright things for all of us.

Epigraph

"The engineer sings as he works—often he only whistles—and in that singing there is the magic of poetry. The engineer's science, like the sailor's chanty, is good literature."

-Scott Buchanan, *Poetry and Mathematics*

Chapter 1

Introduction

Formulating equations of motion for particles in arbitrary flow fields has been an active topic of research for the past 170 years. The problem formally began in the studies of the motion of pendula in air so that more accurate clocks could be developed [18]. This precedes even the governing equations of fluid flow, the Navier-Stokes equations. The full version of the modern equation of motion is complicated and requires large computational resources to numerically simulate. Modern computers make this calculation possible for a wide range of fields. Particulate motion finds application in diverse areas such as pollution control, sedimentation, spray combustion, and biological flows. Because of the wide range of applicability in solving for explicit particle trajectories, mitigating computational burden in simulating particle motion has become an important problem that has been approached by numerous researchers.

1.1 Research Purpose

The equation of motion (EoM) studied here is comprised of a Stokes drag law and the force of gravity. This is a simplification of the rigid sphere equation of motion derived by Maxey and Riley in 1983, and its region of applicability is clarified in Chapter 2. The particle equation of motion is

$$\frac{d\boldsymbol{V}}{dt} = \frac{\boldsymbol{U} - \boldsymbol{V}}{\tau_p} + \boldsymbol{g} \tag{1.1}$$

where $\boldsymbol{V}$ is the particle velocity, $\boldsymbol{U}(\boldsymbol{x}, t)$ is the background flow velocity evaluated at the particle position, and the particle time constant is given by

$$\tau_p = \frac{2r_p^2\rho_p}{9\mu_f}. \tag{1.2}$$

The radius of the particle is r_d, the density of the particle is ρ_p, and the dynamic viscosity of the background fluid is μ_f. For small τ_p, Eq. (1.1) can present a stiff advection problem that is computationally expensive when large numbers of particles are present.

Several researchers have tried to solve these stiffness problems by developing approximate solutions to Eq. (1.1) that are explicit in $\boldsymbol{v}$. Such a solution allows for the calculation of particle velocity without advection of a particle trajectory. The simplest of the v-explicit equations arises from considering the possibility that all the forces on the particle are in balance, i.e. an equilibrium condition.

$$\boldsymbol{V}^{eq} = \boldsymbol{U} + \tau_p \boldsymbol{g}. \tag{1.3}$$

If the equilibrium equation holds, then the velocity of the particle can be determined without propagation of a differential equation. In practice, it is anticipated that in regions away from boundary layers, shear layers, or regions of high vorticity and/or strain, the trajectory defined by the equilibrium EoM is a valid approximation to the full EoM and provides a significant computational advantage over the full expression Eq. (1.1).

The purpose of this work is to gauge the degree of error incurred in using the equilibrium EoM Eq. (1.3) relative to the full expression. The fundamental questions that must be answered are: How does a droplet come to satisfy the equilibrium conditions? What non-dimensional quantity(ies) govern this dynamic? These questions have not been addressed in the literature adequately and are treated here. As will be shown, the value of τ_p provides only part of this information.

1.2 Literature Review

1.2.1 Approximate Equations of Motion

Maxey in 1987 developed a $\boldsymbol{V}$-explicit solution by integrating Eq. (1.1) directly and using integration by parts to expand the solution in powers of τ_p [14]. Neglecting terms proportional to τ_p^2 in the resulting expression produces the solution

$$\boldsymbol{V}^{\text{Maxey}} = \tau_p \boldsymbol{g} + \boldsymbol{U} - \tau_p \left(\frac{\partial \boldsymbol{U}}{\partial t} + (\tau_p \boldsymbol{g} + \boldsymbol{U}) \cdot \nabla \boldsymbol{U} \right). \tag{1.4}$$

If the solution holds, then the particle velocity field $\boldsymbol{V}(\boldsymbol{x}$,t)can be determined in an Eulerian fashion without advection. Maxey used the divergence of this expression to show that particles concentrate in regions of high strain and low vorticity. This buildup and absence of particles in different regions of a flow field is known as preferential concentration.

Druzhinin in 1995 expanded Maxey's solution to a higher order and approximated $\boldsymbol{V}$ by applying the method of successive approximations to Eq. (1.1).

$$\begin{aligned} \boldsymbol{V}^{\text{Druzhinin}} =& \tau_p \boldsymbol{g} + \boldsymbol{U} - \tau_p \left(\frac{\partial \boldsymbol{U}}{\partial t} + (\tau_p \boldsymbol{g} + \boldsymbol{U}) \cdot \nabla \boldsymbol{U} \right) \\ &+ \tau_p^2 \left(\frac{D}{Dt} \frac{D\boldsymbol{U}}{Dt} + \left(\frac{D\boldsymbol{U}}{Dt} \cdot \nabla \right) \boldsymbol{U} + \text{gravity terms} \right) \end{aligned} \tag{1.5}$$

$$\tag{1.6}$$

Note that D/Dt implies a Lagrangian derivative following the fluid, as opposed to d/dt which represents the Lagrangian derivative following the particle. Druzhinin employed this more accurate solution to reduce computational time in studying the interaction of particles on the background flow [3]. Druzhinin demonstrated a reduction of vorticity in particle deficient vortex core regions and increased fluid strain rate in particle concentrated regions such as near hyperbolic stagnation points. This was done through the use of analytical and numerical analysis in flow fields consisting of steady two-dimensional solutions to the Euler equations.

Another solution was introduced by Ferry and Balachandar in 2001 and subsequently improved upon in 2003 by Ferry, Rani, and Balachandar. The solution is based upon a power series expansion of V in terms of the small parameter τ_p, with terms $O\left(\tau_p^3\right)$ neglected [6, 7].

$$\boldsymbol{V}^{\text{Ferry et.al.}} = \boldsymbol{U} - \tau_p \left(\boldsymbol{I} + \tau_p \left(\nabla \boldsymbol{U}\right)^{\mathrm{T}}\right)^{-1} \left(\frac{D\boldsymbol{U}}{Dt} - \boldsymbol{g}\right) \tag{1.7}$$

The solution by Ferry et al. is distinguished from the previous two in that it attempts to make a more accurate prediction of wall-normal migration of particles, which is a result of the advective portion of $d\boldsymbol{V}/dt$. They showed that Eq. (1.7) accurately reproduces all statistical quantities over a set of particles. They also acknowledged that significant errors in the particles location accumulated, despite satisfying these statistical quantities.

1.2.2 Eulerian and Lagrangian Context

The above solutions can be used to determine the error in the equilibrium approximation by taking $\boldsymbol{V}^{Approximation} - (\boldsymbol{U} + \tau_p \boldsymbol{g})$. This provides an idea of which where tracer "ghost" particles deviate significantly from particles with finite inertia in the flow field. This is an Eulerian technique, and has several disadvantages in practice. Actually revealing preferential concentration in the flow still requires evolving a particles position, as the equations provide only velocity. From a physics standpoint, the Eulerian method does not reveal an immediate understanding of how differences between $\boldsymbol{U}$ and $\boldsymbol{V}$ would propagate through time in a given trajectory. It cannot be determined directly from the above equations whether or not errors propagate linearly, exponentially, or otherwise. This is because the flowfield $U(\boldsymbol{x}, t)$ is dependant on x. Since the Eulerian technique requires evolving a particles position to obtain this $\boldsymbol{x}$, the character of these differences might be shown numerically, but is hidden analytically. For instance, spatial gradients in a flow encourage a feedback loop in velocity; small changes in position lead to larger changes in velocity, which lead to larger changes in position, and so on. In order to capture these behaviors numerically, the background flow field data must be updated continually, and the particle time step must remain very small to resolve the updated flowfield.

In contrast, Lagrangian techniques, as discussed in this paper, attempt to directly solve for the path of the flow field, providing explicit expressions for the aforementioned tracer error. Lagrangian techniques can employ Eulerian field equations by inserting a prescribed flow field $U(\boldsymbol{x}, t)$ into the equations of motion and solving the resulting differential equations for the particle position. This will be demonstrated in Chapter 3 for Maxey's equation.

In the general case, the flow field can be treated using a local approximation to expose physical behaviors. To the author's knowledge, Dodin and Elperin were the first to do this in 2004 [2]. The flow field employed was a first order Taylor series expansion given by

$$U_i = U_i|_{\boldsymbol{x}(t=t_o),t=t_o} \left.\frac{\partial U_i}{\partial t}\right|_{\boldsymbol{x}(t=t_o),t=t_o} + \left.\frac{\partial U_i}{\partial x_j}\right|_{\boldsymbol{x}(t=t_o),t=t_o} x_i \tag{1.8}$$

So that the background flow parameters are all constant. From here on, the evaluation of a quantity at an initial particle and time, $U_i|_{\boldsymbol{x}(t=t_o),t=t_o}$, shall be denoted by a superscript as U_i^o. Dodin and Elperin employed the method of successive approximations used by Druzhinin in 1995 to this constructed flow field and obtained the following solution for the particle position using an initial velocity V^o, an initial displacement of zero, and defining $f(t) = (1 - e^{-t/\tau_p})$.

$$\begin{aligned}\boldsymbol{x}_p(t) =& \boldsymbol{U}^o + (U^o - V^o)\, f(t) + (U_t^o + (\nabla U^o)U^o)\left(0.5t^2 - \tau_p t + \tau_p f(t)\right) \\ &+ (\nabla U^o)U^o\,(2\tau_p t - t f(t) + 2\tau_p f(t)) + \boldsymbol{g}\tau_p\,(t - f(t))\end{aligned} \tag{1.9}$$

Further analysis using the local first order Taylor series flow field (1.8) was performed by Mograbi and Bar-Ziv in 2005. They used scaling arguments to show that the local linear flow approximation is valid in a wide range of practical applications. Mograbi and Bar-Ziv constructed the full analytical solution to the problem using state space analysis and drawing conclusions from dynamical system theory [17]. An important feature of this solution is that any particle in a flowfield with spatial dependence is controlled by exponential behavior through time. As a result, Eq. 1.9 by Dodin et al. can only be valid over sufficiently short times since it is a quadratic function of time. They also distinguished between behaviors arising from temporal variation in the flow field against those arising from spatial variation, noting that spatial gradients could lead to nontrivial behaviors through a trajectory such as damped or forced oscillations. Although their solution demonstrated these complex behaviors well, the formulas that Mograbi and Bar-Ziv derive are lengthy and complicated, masking specific physical mechanisms.

1.2.3 The Stokes Number

The particle response time is often made dimensionless by normalizing it with a characteristic time scale of the carrier flow, τ_f. This is known as the Stokes number, *St*.

$$St = \frac{\tau_p}{\tau_f} \tag{1.10}$$

Analytical theory [3], numerical simulations [19, 1], and physical experiments [8], all confirm that the Stokes number plays a vital role in governing the extent to which particles deviate from fluid streamlines. The equilibrium assumption is expected to be valid for small Stokes number, when particles react to slip velocity forces faster than the flow changes.

The characteristic timescale of the carrier flow τ_f can be chosen in a variety of ways. The

carrier flow timescale is sometimes created by dividing a representative length L^* by a representative velocity U^*. For instance, flow approaching a $1m$ diameter cylinder at 2 m/s might be considered to have $\tau_f = 2$s. This technique is useful for characterizing whole particulate flow fields, but is insufficient in capturing the necessary local details of equilibrium analysis because timescales at a given location may be much smaller or larger than the whole flow scale.

The smallest active scales in a turbulent flow are often assumed to be governed by the Kolmogorov scales. In numerical simulations the Kolmogorov time scale is $\tau_\eta = \sqrt{\nu/\varepsilon}$, where ε is the turbulent energy dissipation rate [11, 24]. Using this time scale introduces new difficulties into producing a correct Stokes number. It is based on scaling arguments, and is not precise. The winding modes observed by Mograbi and Bar-Ziv could produce flow conditions with intense variation in ε that maintain a trajectory close to equilibrium. The turbulent energy dissipation rate is typically listed as an average over a flowfield and used as a measure in homogeneous isotropic turbulence. Also, evaluating equilibrium based on the Stokes number is an Eulerian technique and suffers from the same setbacks as the three approximate Eulerian solutions.

1.2.4 Outline of Thesis

The next chapter derives the conditions where Eq. (1.1) is valid so that the range of applicability of this analysis is well understood. The equations of motion of interest are then formulated based on a first-order Taylor series expansion of the flow field. Lagrangian analysis of particle trajectories is conducted using analytical flow fields to reveal the important parameters leading to discrepancy from equilibrium. This is done in temporal and spatial cases and different mechanisms are shown to govern each. In the general cases of one, two, and three dimensions, the relation between the equilibrium solution and the full solution is derived and the governing parameters are defined. A numerical simulation is conducted to demonstrate how equilibrium can be predicted based on this relationship. An Eulerian viewpoint is then derived and the relation between it and the Lagrangian solutions are discussed.

Chapter 2

Mathematical Description and Range of Applicability

The basis for the particle equation of motion is the extensively used rigid sphere equation of motion owed to Maxey and Riley [13].
The equation is of motion is:

$$m_s \frac{d\boldsymbol{V}(t)}{dt} = \underbrace{(m_s - m_f)\,\boldsymbol{g}}_{\text{Buoyancy}} + \underbrace{m_f \frac{D\boldsymbol{U}(\boldsymbol{x}_s(t),t)}{Dt}}_{\text{Pressure Gradient}} \tag{2.1}$$

$$- \frac{1}{2} m_f \frac{d}{dt}\left(\boldsymbol{V}(t) - \boldsymbol{U}(\boldsymbol{x}_s(t),t) - \frac{1}{10} r_s^2 \nabla^2 \boldsymbol{U}(\boldsymbol{x}_s(t),t)\right) \quad \text{(Added Mass)} \tag{2.2}$$

$$- \frac{6\pi r_s^2 \mu_f}{\sqrt{\pi \nu_f}} \int_0^t \frac{\frac{d}{dt^*}\left(\boldsymbol{V}(t^*) - \boldsymbol{U}(\boldsymbol{x}_s(t^*),t^*) - \frac{1}{6} r_s^2 \nabla^2 \boldsymbol{U}(\boldsymbol{x}_s(t^*),t^*)\right)}{\sqrt{t - t^*}} dt^* \quad \text{(History Integral)}$$

$$- 6\pi r_s \mu_f \left[\boldsymbol{V}(t) - \boldsymbol{U}(\boldsymbol{x}_s(t),t) - \frac{1}{6} r_s^2 \nabla^2 \boldsymbol{U}(\boldsymbol{x}_s(t),t))\right] \quad \text{(Stokes Drag)} \tag{2.3}$$

All background fluid quantities are evaluated at the position of the sphere $\boldsymbol{x_s}(t) = \boldsymbol{x_s}(0) + \int_0^t \boldsymbol{v_s}(t*)dt*$. The mass of the rigid sphere is m_s and the mass of a sphere volume of carrier fluid is m_f. There are two different derivatives present. D/Dt is the derivative following the fluid, and d/dt is the derivative following the sphere. The equation's most limiting assumption imposes creeping flow around the sphere, so that the advective terms in the Navier-Stokes equations may be neglected. The Reynold's number for flow around the sphere, defined as $Re_p = r_p\left(\boldsymbol{U} - \boldsymbol{V}\right)/\nu_f$, must be much less than 1. Although the equation is formulated for a rigid sphere, it may be used for droplets in instances where droplet to fluid density ratios are high (for instance, liquid spray in air) [21].

The ∇^2 terms are collectively known as the Faxen corrections [5], and account for a nonuniform fluid velocity field across the radius of the particle. If the particle diameter is small compared

to the surrounding flow structures, then these terms can be neglected. For most engineering applications, this assumption holds. One important exception is near boundary layer regions, where the local flow gradients may often be on the scale of the particle size. This can induce a lift force due to particle rotation that must be accounted for with another term [20]. The history integral arises from the diffusion of vorticity around the sphere, and the added mass term is a consequence of accelerating the flow around the particle to accommodate the no-slip boundary condition. The pressure gradient term represents the force that would be required to accelerate the volume of fluid that the particle displaces. The stokes drag is the steady-state drag corresponding to the instantaneous velocity.

A review by Michaelides [16] states that the history integral may be neglected for particle-to-fluid density ratios of 250 and higher for an arbitrary flow field. This result is in agreement with several other studies [12, 23]. The history integral's magnitude decays through time in relation to the other terms. Approximations to the history integral in low frequency flows have shown that its significance decays as $t^{-1/2}$ initially and t^{-2} at longer times [15]. Ultimately what is insignificant is a decision made by the user, so some authors have advocated evaluating the significance of the history integral *a posteriori* by evaluating the trajectory of a single particle through the largest gradient portions of the given flow field [9]. The particles and droplets studied here satisfy $\rho_p/\rho_f \gg 1$, and are referred to as heavy particles. The Faxen terms and the history integral are removed, leaving

$$\left(m_p + \frac{1}{2}m_f\right)\frac{d\boldsymbol{V}}{dt} = (m_p - m_f)\,\boldsymbol{g} + m_f\frac{D\boldsymbol{U}(\boldsymbol{x}_s,t)}{dt} + \frac{1}{2}m_f\frac{d\boldsymbol{U}(\boldsymbol{x}_s,t)}{dt} - 6\pi r_p\mu_f\left(\boldsymbol{V} - \boldsymbol{U}(\boldsymbol{x}_s,t)\right). \tag{2.4}$$

A dimensional analysis shows that the difference between $D\boldsymbol{U}/Dt$ and $d\boldsymbol{U}/dt$ is of the same magnitude as the advective terms in the Navier-Stokes equations that have already been neglected [16, 9]. Therefore, $D\boldsymbol{U}/Dt$ and $d\boldsymbol{U}/dt$ can be equated, giving

$$\left(m_p + \frac{1}{2}m_f\right)\frac{d\boldsymbol{V}}{dt} = (m_p - m_f)\,\boldsymbol{g} + \frac{3}{2}m_f\frac{d\boldsymbol{U}}{dt} - 6\pi r_p\mu_f\left(\boldsymbol{V} - \boldsymbol{U}\right). \tag{2.5}$$

For a heavy particle $m_p \gg m_f$ so that the added mass term $m_f d\boldsymbol{U}/dt$ is negligible. Removing the added mass term and then exchanging mass for density and r_p yields

$$\frac{d\boldsymbol{V}}{dt} = \frac{9\mu_f}{2r_p^2\rho_p}\left(\boldsymbol{U} - \boldsymbol{V}\right). \tag{2.6}$$

Inserting the definition of the particle time constant, Eq. (1.2), is the final step in reducing the full equation of motion to the heavy particle equation of motion (1.1).

In order to analytically evaluate the dynamics of the system, we evaluate $\boldsymbol{U}(\boldsymbol{x}(t),t)$ as a first-order Taylor series expansion at a certain time about a point $\boldsymbol{x}_p$, which is the particle position.

The expansion is given by

$$\boldsymbol{U}\left(\boldsymbol{x}_p(t),t\right)=\boldsymbol{U}\left(\boldsymbol{x}_p(t_o),t_o\right)+\nabla\boldsymbol{U}\left(\boldsymbol{x}_p(t_o),t_o\right)\cdot\left(\boldsymbol{x}_p(t)-\boldsymbol{x}_p(t_o)\right)+\frac{\partial\boldsymbol{U}\left(\boldsymbol{x}_p(t_o),t_o\right)}{\partial t}\left(t-t_o\right)$$
$$+O(d\boldsymbol{x}_p^2)+O(dt^2)+O(d\boldsymbol{x}_p dt). \tag{2.7}$$

The difference in position is written as $\boldsymbol{x}_p(t)-\boldsymbol{x}_p(t_o)=\Delta\boldsymbol{x}_p$ so that we can define

$$\boldsymbol{V}=\frac{d\Delta\boldsymbol{x}_p}{dt}. \tag{2.8}$$

Using this definition the Taylor expansion can be succinctly combined with Eq. (1.1) yielding

$$\frac{d^2}{dt^2}\Delta\boldsymbol{x}_p+\frac{1}{\tau_p}\frac{d}{dt}\Delta\boldsymbol{x}_p=\frac{1}{\tau_p}\left[\boldsymbol{U}(\boldsymbol{x}_p(0),0)+\nabla\boldsymbol{U}\cdot\Delta\boldsymbol{x}_p+\frac{d\boldsymbol{U}(\boldsymbol{x}_p(0),0)}{dt}\Delta t\right]+\boldsymbol{g}. \tag{2.9}$$

The equilibrium droplet displacement, $\Delta\boldsymbol{x}_p^{eq}$, can be obtained from Eq. (1.3) to give

$$\frac{d}{dt}\Delta\boldsymbol{x}_p^{eq}=\boldsymbol{U}\left(\boldsymbol{x}_p(0),0\right)+\nabla\boldsymbol{U}\cdot\Delta\boldsymbol{x}_p^{eq}+\frac{d\boldsymbol{U}\left(\boldsymbol{x}_p(0),0\right)}{dt}\Delta t+\boldsymbol{g}\tau_p. \tag{2.10}$$

From here onward, Δt shall be written as t, since the initial time can always considered to be zero. The objective is to characterize the conditions under which the droplet achieves or departs from a dynamic equilibrium state throughout its trajectory given the following:

1. Initial slip velocity
2. Background flow characteristics
3. Time and space over which the flow can be treated as a linearized Taylor series expansion

We denote this time and space region as $\mathbb{R}^4_{\text{lin}}$. The Taylor series is not a restriction on the types of flow fields that this analysis can be applied to. Once the droplet leaves $\mathbb{R}^4_{\text{lin}}$, the Taylor series expansion can be evaluated at the new point.

The spatial coupling in Eq.'s (2.9) and (2.10) produces complicated solutions that make analysis of the underlying physics difficult. Two simple cases that avoid this problem are a purely temporal flow field and a one-dimensional flow field. Both are now presented in order to clearly show the dynamics leading to equilibrium. An analysis of the higher dimensional solutions is then given which avoids explicitly accounting for every term in the solutions, leading to a simple guideline for evaluating the equilibrium condition.

Chapter 3

Demonstrations of Equilibrium Physics

3.1 Purely Temporal Flow Field

If the background flow field is purely a function of time $\boldsymbol{u}(t)$ then each direction is independent and the equation for each V_i takes the form

$$\frac{dV}{dt} + \frac{V}{\tau_p} = \frac{U(t)}{\tau_p} + g \tag{3.1}$$

with the equilibrium equation satisfying

$$V^{eq} = U(t) + g\tau_p \tag{3.2}$$

Equation (3.1) can be directly integrated (using the integrating factor method) to produce

$$\int \frac{d}{dt} e^{t/\tau_p} V dt = \int e^{t/\tau_p} \frac{U(t)}{\tau_p} dt + \int e^{t/\tau_p} g dt \tag{3.3}$$

$$e^{t/\tau_p} (V - V_o) = \int e^{t/\tau_p} \frac{U(t)}{\tau_p} dt + \int e^{t/\tau_p} g dt \tag{3.4}$$

The integral involving $U(t)$ can be expanded by parts using the formulation $\int u dv = uv - \int v du$ with

$$u = U(t)/\tau_p \qquad dv = e^{t/\tau_p} dt \tag{3.5}$$

$$du = U'(t)/\tau_p dt \qquad v = \tau_p e^{t/\tau_p} \tag{3.6}$$

The integral is taken from $t^* = 0$ to $t^* = t$

$$e^{t/\tau_p}\left(V - V_o\right) = U(t)e^{t/\tau_p} - U_o + g\tau_p\left(e^{t/\tau_p} - 1\right) - \int e^{t/\tau_p}U'(t)dt \tag{3.7}$$

Now, the parts expansion is used on the integral again to continue expanding in powers of τ_p

$$u = U'(t) \qquad dv = e^{t/\tau_p}dt \tag{3.8}$$

$$du = U''(t)dt \qquad v = \tau_p e^{t/\tau_p} \tag{3.9}$$

Leaving the integral as

$$\int_0^t e^{t^*/\tau_p}U'(t^*)dt^* = \tau_p U'(t)e^{t/\tau_p} - \tau_p U'(0) - \int \tau_p e^{t/\tau_p}U''(t)dt \tag{3.10}$$

If this process of expanding the remaining integral is continued indefinitely we arrive at

$$e^{t/\tau_p}\left(V - V_o\right) = +g\tau_p\left(e^{t/\tau_p} - 1\right) + \sum_{i=0}^{\infty}(-1)^i\tau_p^i\left(e^{t/\tau_p}\frac{d^{(i)}(U)(t)}{dt} - \frac{d^{(i)}(U)(0)}{dt}\right) \tag{3.11}$$

Dividing the exponential through, and expanding the $i = 0$ term in the sum gives

$$V = \underbrace{U(t) + g\tau_p}_{V^{eq}} + V_o e^{-t/\tau_p} - U_o e^{-t/\tau_p} - ge^{-t/\tau_p} + \sum_{i=1}^{\infty}(-1)^i\tau_p^i\left(\frac{d^{(i)}(U)(t)}{dt} - e^{-t/\tau_p}\frac{d^{(i)}(U)(0)}{dt}\right) \tag{3.12}$$

The series converges at any point in time for bounded $U(t)$ and $\tau_p < 1$. Thus we can expect that for temporal cases, errors in equilibrium are associated with products of the time constant and background derivatives that grow in power and order respectively. Secondary errors are the decaying effects associated with initial slip velocity and finite flow derivatives of order 1 and higher. These errors quickly become negligible for $t > 3\tau_p$.

3.2 Linear Temporal Flow Field

The temporal flow field can be analyzed locally using a Taylor series expansion. An n-th order polynomial flow field will have equilibrium deviation terms up to $\tau_p^n d^n U/dt^n$ according to Eq. (3.12) The solution to the first order linearized temporal flow field is obtained by inserting $U(t) = U_o + U_t t$ into 3.12. This solution is given the notation V^{Ut}.

$$V^{U_t} = U_o + U_t t + g\tau_p\left(1 - e^{-t/\tau_p}\right) + \left(V_o - U_o\right)e^{-t/\tau_p} - U_t\tau_p\left(1 - e^{-t/\tau_p}\right) \tag{3.13}$$

$$= U_o + tU_t + g\tau_p - U_t\tau_p + e^{-t/\tau_p}\left(V_o - U_o - g\tau_p + U_t\tau_p\right) \tag{3.14}$$

The corresponding equilibrium solution is

$$V^{U_t Eq} = U_o + U_t t + g\tau_p. \tag{3.15}$$

Comparing equations (3.13) and (3.15), we see that even after the transient terms decay away, the velocity error between the full and equilibrium solution has a constant bias of $U_t\tau_p$.

Integrating (3.13) and (3.15) gives the position $\Delta X_p^{U_t}$ and the equilibrium position $\Delta X_p^{U_t Eq}$ (note that $\int_0^t e^{-t^*/\tau_p} dt^* = \tau_p - \tau_p e^{-t/\tau_p}$)

$$\Delta X_p^{U_t} = U_o t + g\tau_p t + U_t \frac{t^2}{2} + \tau_p \left(V_o - U_o - g\tau_p\right)\left(1 - e^{-t/\tau_p}\right) \tag{3.16}$$

$$- \tau_p U_t t + \tau_p^2 U_t \left(1 - e^{-t/\tau_p}\right) \tag{3.17}$$

$$\Delta X_p^{U_t Eq} = U_o t + g\tau_p t + U_t \frac{t^2}{2} \tag{3.18}$$

so that the difference is

$$\Delta X_p^{U_t} - \Delta X_p^{U_t Eq} = \tau_p \left(V_o - U_o - g\tau_p\right)\left(1 - e^{-t/\tau_p}\right) - \tau_p U_t t + \tau_p^2 U_t \left(1 - e^{-t/\tau_p}\right). \tag{3.19}$$

The equilibrium discrepancy includes the decaying slip velocity terms, a linearly growing spatial difference, and a constant bias of $U_t\tau_p^2$. This equation will be useful in characterizing how temporal errors correlate to spatial errors in the subsequent analysis of one-dimensional and three-dimensional flow fields.

3.3 One-Dimensional Flow

The one-dimensional flow field is constructed using the flow conditions local to the particle position, which is given by Eq. (2.7). Neglecting the second order terms in the expansion and considering a single direction defines the one-dimensional flow field as

$$U(x_p, t) = U(x_p(0), 0) + U_x(x_p(0), 0)\left[x_p(t) - x_p(0)\right] + U_t(x_p(0), 0)t = U^o + U_x^o \Delta x_p + U_t^o t. \tag{3.20}$$

Under this framework the equation of motion becomes

$$\left(\frac{d^2}{dt^2} + \frac{1}{\tau_p}\frac{d}{dt}\right)\Delta x_p = \frac{1}{\tau_p}\left[U^o + U_x^o \Delta x_p + U_t^o t\right] + g. \tag{3.21}$$

An arbitrary initial velocity and zero initial displacement provide the following initial conditions.

$$\Delta x_p(0) = \Delta x_p^{eq}(0) = 0 \tag{3.22}$$

$$\frac{d\left(\Delta x_p(0)\right)}{dt} = V^o.$$

The full solution for the path trajectory $\Delta x_p(t)$ is derived using these initial conditions.

$$\Delta x_p^F = -\mathbb{Q} - \frac{U_t}{U_x}t + \left[\frac{\mathbb{Q}}{2} + \frac{1}{\sqrt{1+4U_x\tau_p}}\left(\frac{\mathbb{Q}}{2} + \frac{U_t\tau_p}{Ux} + V_o\tau_p\right)\right] e^{\frac{-1+\sqrt{1+4U_x\tau_p}}{2\tau_p}t}$$
$$+ \left[\frac{\mathbb{Q}}{2} - \frac{1}{\sqrt{1+4U_x\tau_p}}\left(\frac{\mathbb{Q}}{2} + \frac{U_t\tau_p}{Ux} + V_o\tau_p\right)\right] e^{\frac{-1-\sqrt{1+4U_x\tau_p}}{2\tau_p}t} \tag{3.23}$$

Here the constant particular solution terms are defined for convenience as

$$\mathbb{Q} = \left(\frac{g\tau_p}{U_x^o} + \frac{U_t^o}{U_x^{o2}} + \frac{U^o}{U_x^o}\right) \tag{3.24}$$

The detailed description of the solution procedure that provides Eq. (3.23) can be found in Appendix A. The equilibrium trajectory satisfies

$$\frac{d}{dt}\Delta x_p^{eq} = U^o + U_x^o\Delta x_p + U_t^o t + g. \tag{3.25}$$

Note the equilibrium equation is first-order and uses only the zero-displacement initial condition. The equilibrium solution is

$$\Delta x_p^{eq}(t) = \mathbb{Q}e^{U_x^o t} - \frac{U_t^o}{U_x^o}t - \mathbb{Q}. \tag{3.26}$$

One important characteristic of these governing equations is that the exponential terms are dominated by the spatial variations, with temporal variation only seen in coefficients and linear terms.

The physical mechanism for this is that spatial variations allow a given particle trajectory to influence the background flow field that the particle sees. The physical mechanism for this is that changes in the particle position affect the background velocity that the particle sees when spatial gradients are present, and this behavior is reinforced through time. For example, if U_x is positive, a small positive change in Δx_p will lead to larger background velocities, which will in turn drive larger positive changes in Δx_p. This feedback loop produces an exponential process. The temporal variations produce uniform growth (as opposed to feedback growth) in U_x and Δx_p.

The quantity $U_x\tau_p$ is critical in describing the behavior of the equations. It will be shown that it is the most important parameter in describing how the full solution relates to equilibrium. $U_x\tau_p$ is a ratio of the relaxation time of the particle to the fluid spatial variation timescale, and is a more accurate depiction of what the traditional Stokes number tries to represent for spatially varying flows. Thus, the one-dimensional Stokes number for heavy particles is defined as

$$\boxed{St = U_x\tau_p} \tag{3.27}$$

An interesting feature of this Stokes number is that it does not include temporal variations into the timescale for background fluid variation. Since spatial variations and temporal variations affect particle motions in different ways (exponentially and linearly), temporal effects must be understood and accounted for separately.

Insight into how $\Delta x_p^F(t)$ is related to $\Delta x_p^{eq}(t)$ can be obtained by using $4U_x\tau_p$ as a small parameter to expand the exponential terms as

$$\sqrt{1+4U_x^o\tau_p} = 1 + 2U_x^o\tau_p - \frac{\left(4U_x^o\tau_p\right)^2}{8} + \frac{\left(4U_x^o\tau_p\right)^3}{16} + \cdots . \tag{3.28}$$

A hierarchy of solutions based on this expansion is developed, denoting Δx_p^{A1} as the first-order solution that retains two terms, Δx_p^{A2} as the second order solution that retains three terms, and so forth. The approximations are formed by direct substitution of Eq. (3.28) into the full solution Eq. (3.23) wherever the term $\sqrt{1+4U_x^o\tau_p}$ appears. This leaves the the first, second, and third order approximations as

$$\begin{aligned}\Delta x_p^{A1} = &-\mathbb{Q} - \frac{U_t}{U_x}t + \left[\frac{\mathbb{Q}}{2} + \frac{1}{1+2U_x\tau_p}\left(\frac{\mathbb{Q}}{2} + \frac{U_t\tau_p}{U_x} + V_o\tau_p\right)\right]e^{U_x t} \\ &+ \left[\frac{\tau_p\left(U_o + g\tau_p - V_o\right)}{1+2U_x\tau_p}\right]e^{-(t/\tau_p + U_x)t}\end{aligned} \tag{3.29}$$

$$\begin{aligned}\Delta x_p^{A2} = &\left[\frac{\mathbb{Q} + \tau_p\left(V_o + U_o + g\tau_p\right) + 2\tau_p U_t/U_x + U_x\tau_p\left(-g\tau_p^2 - U_o\tau_p\right) - U_t\tau_p^2}{1 + 2U_x\tau_p - 2U_x^2\tau_p^2}\right]e^{\left(U_x - U_x^2\tau_p\right)t} \\ &+ \left[\frac{\tau_p\left(U_o + g\tau_p - V_o\right) - U_x\tau_p\left(g\tau_p^2 + U_o\tau_p\right) - U_t\tau_p^2}{1 + 2U_x\tau_p - 2U_x^2\tau_p^2}\right]e^{\left(-1/\tau_p - U_x + \tau_p U_x^2\right)t} - \mathbb{Q} - \frac{U_t}{U_x}t\end{aligned} \tag{3.30}$$

$$\begin{aligned}\Delta x_p^{A3} = &-\mathbb{Q} + \frac{U_t}{U_x}t + \\ &\left[\frac{\mathbb{Q} + \tau_p\left(U_o + V_o + g\tau_p\right) + 2\tau_p U_t/U_x - U_t\tau_p^2 + U_x\tau_p\left(-U_o\tau_p - g\tau_p^2 + 2U_t\tau_p^2\right) + U_x^2\tau_p^2\left(2U_o\tau_p + 2g\tau_p^2\right)}{1 + 2U_x\tau_p - 2U_x^2\tau_p^2 + 4U_x^3\tau_p^3}\right]e^{\left(U_x - U_x^2\tau_p + 2U_x^3\tau_p^2\right)t} \\ &+\left[\frac{\tau_p\left(U_o + g\tau_p - V_o\right) - U_t\tau_p^2 + U_x\tau_p\left(-U_o\tau_p - g\tau_p^2 + 2U_t\tau_p^2\right) + U_x^2\tau_p^2\left(2U_o\tau_p + 2g\tau_p^2\right)}{1 + 2U_x\tau_p - 2U_x^2\tau_p^2 + 4U_x^3\tau_p^3}\right]e^{\left(-1/\tau_p - U_x + U_x^2\tau_p - 2U_x^3\tau_p^2\right)t}\end{aligned} \tag{3.31}$$

The solutions all share the same linear terms as well as fast decaying exponential term. Notice that the higher order exponential coefficients contain corrective terms in powers of $U_x\tau_p$ as well as temporal terms like $U_t\tau_p^2$ that do not appear in x_p^{A1}

The lagrangian error between Δx_p^{A1} and Δx_p^{eq} can be evaluated directly:

$$\Delta x_p^{A1} - \Delta x_p^{eq} = \left[\frac{\tau_p\left(V_o - U_o - g\tau_p\right)}{1+2U_x\tau_p}\right]e^{U_x t} - \left[\frac{\tau_p\left(V_o - U_o - g\tau_p\right)}{1+2U_x\tau_p}\right]e^{-(t/\tau_p + U_x)t} \tag{3.32}$$

The differences from equilibrium in the higher order solutions are also easily analyzed if the differences in the exponential powers are considered to be negligible. This reveals some of the effects that the higher order solutions capture.

$$\Delta x_p^{A2} - \Delta x_p^{eq} = \left[\frac{\tau_p\left(V_o - U_o - g\tau_p\right) + U_x\tau_p\left(U_o\tau_p + g\tau_p^2\right) + U_t\tau_p^2}{1 + 2U_x\tau_p - 2U_x^2\tau_p^2}\right] e^{U_x t - \tau_p U_x^2 t}{}^{0}$$
$$+ \left[\frac{\tau_p\left(U_o + g\tau_p - V_o\right) - U_x\tau_p\left(g\tau_p^2 + U_o\tau_p\right) - U_t\tau_p^2}{1 + 2U_x\tau_p - 2U_x^2\tau_p^2}\right] e^{\left(-1/\tau_p - U_x + \tau_p U_x^2\right)t} \tag{3.33}$$

$$\Delta x_p^{A3} - \Delta x_p^{eq} =$$
$$\left[\frac{\tau_p(V_o - U_o - g\tau_p) + U_t\tau_p^2 + U_x\tau_p\left(U_o\tau_p + g\tau_p^2 - 2U_t\tau_p^2\right) - U_x^2\tau_p^2\left(2U_o\tau_p + 2g\tau_p^2\right)}{1 + 2U_x\tau_p - 2U_x^2\tau_p^2 + 4U_x^3\tau_p^3}\right] e^{(U_x - U_x^2\tau_p + 2U_x^3\tau_p^2)t}{}^{0}$$
$$+\left[\frac{\tau_p\left(-V_o + U_o + g\tau_p\right) - U_t\tau_p^2 + U_x\tau_p\left(-U_o\tau_p - g\tau_p^2 + 2U_t\tau_p^2\right) + U_x^2\tau_p^2\left(2U_o\tau_p + 2g\tau_p^2\right)}{1 + 2U_x\tau_p - 2U_x^2\tau_p^2 + 4U_x^3\tau_p^3}\right] e^{\left(\frac{-1}{\tau_p} - U_x + U_x^2\tau_p - 2U_x^3\tau_p^2\right)t} \tag{3.34}$$

Slip velocity errors can be seen in each solution. The Lagrangian derivative of the fluid following itself, $DU/Dt = U_t + U_oU_x$, is also seen weighted by τ_p^2 in x_p^{A2}. The pattern does not continue into x_p^{A3} however (there is no DU/Dt^2 term present). Instead, the consistency of powers of $U_x\tau_p$ with separate temporal effects is seen in x_p^{A3}.

The error in the first order approximation, Eq. (3.32), has no dependance on U_t. Physically, this is incorrect. In section 3.1 purely temporal velocity errors were shown to scale as $U_t\tau_d$, and similar behavior must be present in the spatial case. The first order approximation masks the temporal behavior, which is demonstrated through the following limits.

$$\lim_{U_x\to 0}\Delta x_p^{A1} = U_o t + g\tau_p t + U_t\frac{t^2}{2} + \tau_p\left(V_o - U_o - g\tau_p\right)\left(1 - e^{-t/\tau_p}\right) \tag{3.35}$$

$$\lim_{U_x\to 0}\Delta x_p^{eq} = U_o t + g\tau_p t + U_t\frac{t^2}{2} \tag{3.36}$$

$$\lim_{U_x\to 0}\Delta x_p^{F} = \lim_{U_x\to 0}\Delta x_p^{A2} = \lim_{U_x\to 0}\Delta x_p^{A3} = \Delta x_p^{Ut} =$$
$$U_o t + g\tau_p t + U_t\frac{t^2}{2} + \tau_p\left(V_o - U_o - g\tau_p\right)\left(1 - e^{-t/\tau_p}\right) - U_t\tau_p t + U_t\tau_p^2\left(1 - e^{-t/\tau_p}\right) \tag{3.37}$$

The technique for evaluating these limits is demonstrated in Appendix B. In this limit the first order solution is missing the $U_t\tau_p t$ and $U_t\tau_p^2$ terms in the full solution. The second and third order solutions account for these temporal effects.

In order for gravitational forces to be accounted for, τ_p must be finite. This means that the proper limit of the Stokes number approaching zero is the limit $U_x \to 0$, which is "assisted"

through the presence of a small τ_p. Even for vanishingly small Stokes number, there are still finite temporal errors between equilibrium and the full solution.

3.3.1 Maxey's Solution

As noted before, other authors have derived approximate solutions to the droplet equation of motion that are explicit in $\boldsymbol{v}$. Maxey's solution [14] is particularly interesting in the scope of this work, and is denoted Δx_p^M. In the present notation, his solution is given by

$$\frac{d\Delta \boldsymbol{x}_p^M}{dt} = \tau_p \boldsymbol{g} + \boldsymbol{U} - \tau_p \left(\frac{\partial \boldsymbol{U}}{\partial t} + (\tau_p \boldsymbol{g} + \boldsymbol{U}) \cdot \nabla \boldsymbol{U} \right). \tag{3.38}$$

Note that all quantities in the equation are evaluated at the particle location. The imposed condition is neglect of initial transient term by allowing zero initial slip velocity. Here Maxey's derivation is modified to include an arbitrary initial velocity. This solution is given by

$$\begin{aligned} &\frac{d\Delta \boldsymbol{x}_p^{M+IC}}{dt} = \left(\boldsymbol{V}^o - \boldsymbol{U}^o - \tau_p \boldsymbol{g}\right) e^{-t/\tau_p} + \tau_p \boldsymbol{g} + \boldsymbol{U} \\ &-\tau_p \left(\frac{d\boldsymbol{U}}{dt} + \left(\left(\boldsymbol{V}^o - \boldsymbol{U}^o - \tau_p \boldsymbol{g}\right) e^{-t/\tau_p} + \tau_p \boldsymbol{g} + \boldsymbol{U} \right) \cdot \nabla \boldsymbol{u} \right). \end{aligned} \tag{3.39}$$

Recognizing that $\tau_p \boldsymbol{g} + \boldsymbol{u}$ is the equilibrium solution velocity, this formula supports $Ux\tau_p$ Stokes number metric accompanied with τ_p weighted temporal variations. To put these equations in the same framework defined above, the linear flow field (3.20) is inserted into (3.38) and (3.39), resulting in

$$\Delta x_p^M(t) = (\mathbb{Q}) \frac{1}{1 - U_x^o \tau_p} e^{\left(U_x^o - U_x^{o2} \tau_p\right) t} - \mathbb{Q} - \frac{U_t^o}{U_x^o} t \tag{3.40}$$

and

$$\begin{aligned} \Delta x_p^{M+IC}(t) = &\frac{\tau_p \left(1 - U_x^o \tau_p\right) \left(U^o - V^o + g\tau_p\right)}{1 + U_x^o \tau_p - U_x^{o2} \tau_p^2} e^{-t/\tau_p} - \mathbb{Q} \\ &- \frac{U_t^o}{U_x^o} t + \left(\mathbb{Q} - \frac{\tau_p \left(1 - U_x^o \tau_p\right) \left(U^o - V^o + g\tau_p\right)}{1 + U_x^o \tau_p - U_x^{o2} \tau_p^2} \right) e^{\left(U_x^o - U_x^{o2} \tau_p\right) t}. \end{aligned} \tag{3.41}$$

Due to the imposed initial equilibrium condition and the neglect of transient terms in (3.38), $\Delta x_p^M(0)$ cannot be independently adjusted. This introduces a difficulty when comparing with previous solutions. The modified solution Δx_p^{M+IC} (Maxey + initial conditions) circumvents this problem.

3.3.2 Equation of Motion Error Demonstration

The set of solutions Δx_p^F, Δx_p^{A1}, Δx_p^{A2}, Δx_p^{eq}, Δx_p^M, and Δx_p^{M+IC} are compared as follows; The background flow is specified as

$$U = U_o + U_x^o x + U_t^o t. \tag{3.42}$$

Note that U_o is a constant bias velocity whereas U^o is $U(x_p(0), 0)$. Using this flow field, droplets are equally distributed through $x \in (0, 3)$ with an initial non-zero slip velocity and advected through time using the above solutions. The flow field setup is depicted in figure 3.1

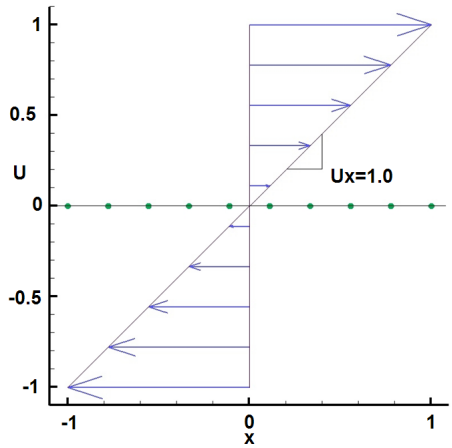

Figure 3.1: One dimensional flow field setup for positive U_x. Initial particle positions are green dots.

For positive U_x^o, the velocity field drives droplets away from the origin ($U_t = 0$) or from a moving point in the case of $U_t \neq 0$. Errors are exacerbated with increasing distance from the origin and with time. If U_x^o is negative, over long times the solutions converge to a point that can be stationary ($U_t = 0$) or dynamic ($U_t \neq 0$).

The quantity of interest is the trajectory discrepancy between the approximate and full solutions, for instance $\Delta x_p^F - \Delta x_p^{eq}$. This discrepancy is normalized by

$$\frac{1}{x_{\max} - x_{\min}} \int_{x_{\min}}^{x_{\max}} u(x,t)dx \tag{3.43}$$

where x_{min} and x_{max} are the leftmost and rightmost points in the domain. A typical plot of this kind is shown in Figure 3.2. Note the improved agreement with the full solution as the order of approximation is increased. The equilibrium prediction is comparable in quality to Maxey's original equation, and the first-order approximation.

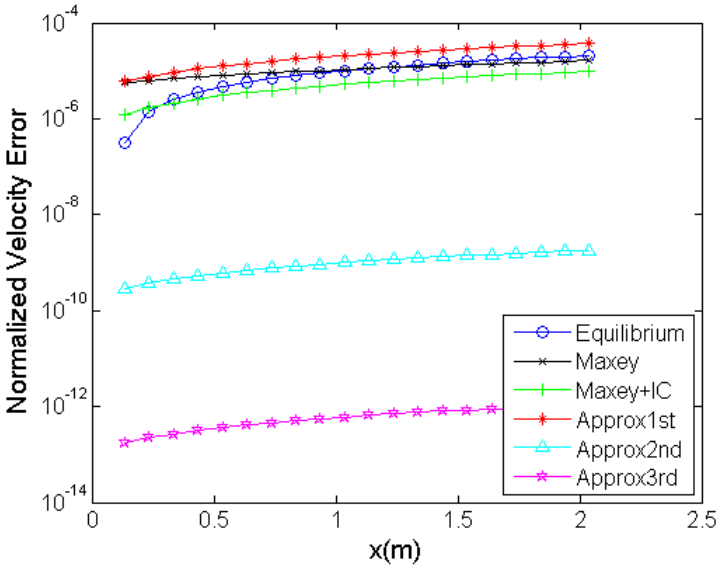

Figure 3.2: Discrepancy between approximate solutions and the full droplet EoM. Parameters are: $U_x^o = -0.5s^{-1}$, $U^o - V^o = 0.10$ m/s, $t = 0.8$ s, $\tau_p = 4.9\text{x}10^{-5}$s, $4U_x^o\tau_p = -9.8\text{x}10^{-5}$, $U_o = 0.0$ m/s, $U_t^o = 0.0$ m/s^2

The solutions in the hierarchy cannot be guaranteed to be more accurate than other solutions for all conditions. This is a result of oscillatory modes that occur when particles repeatedly pass up and then fall behind the flow field. In almost all cases, the accuracy of the hierarchy is best represented by Figure 3.3 below.

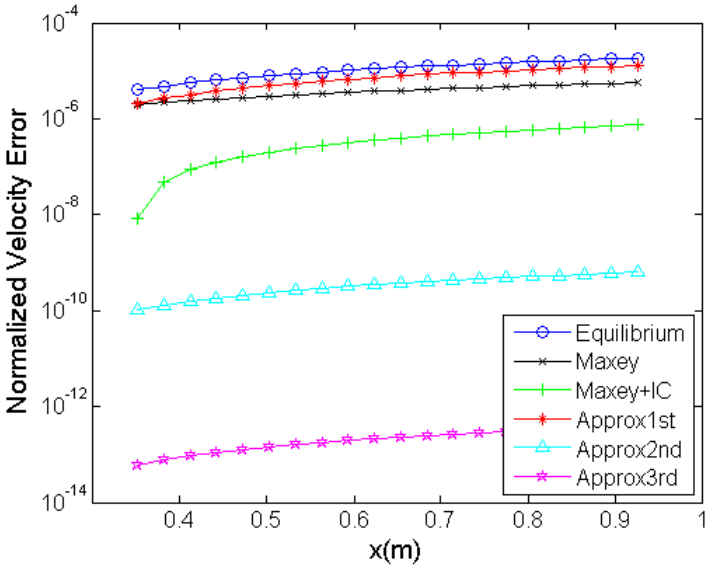

Figure 3.3: Representative hierarchy accuracy. Parameters are: $U_x^o = -0.5s^{-1}$, $U^o - V^o = 0.10$ m/s, $t = 3.2$ s, $\tau_p = 4.9\text{x}10^{-5}$s, $4U_x^o\tau_p = -9.8\text{x}10^{-5}$, $U_o = 0.0$ m/s, $U_t^o = 0.0$ m/s^2

3.3.3 Spatial Departures

In order to demonstrate the role of the spatial gradients, the temporal gradient U_t^o is set to 0 for the moment. All solutions have increasing error with increasing values of Stokes number. This is shown graphically in Figures 3.4 through 3.6. In each of the following figures, the value of $4U_x^o\tau_p$ is incremented systematically.

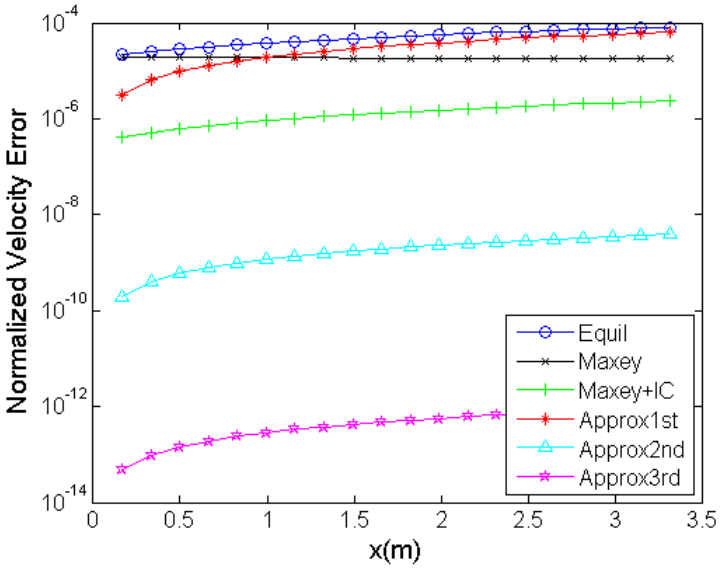

Figure 3.4: Performance of the approximate solutions for $4U_x^o\tau_p = 1.22\text{x}10^{-4}$. Parameters are: $U_x^o = 0.1s^{-1}$, $U^o - V^o = 0.10$ m/s, $t = 1.0$ s, $\tau_p = 3.1\text{x}10^{-4}$s, $U_o = 0.0$ m/s, and $U_t^o = 0.0$ m/s^2

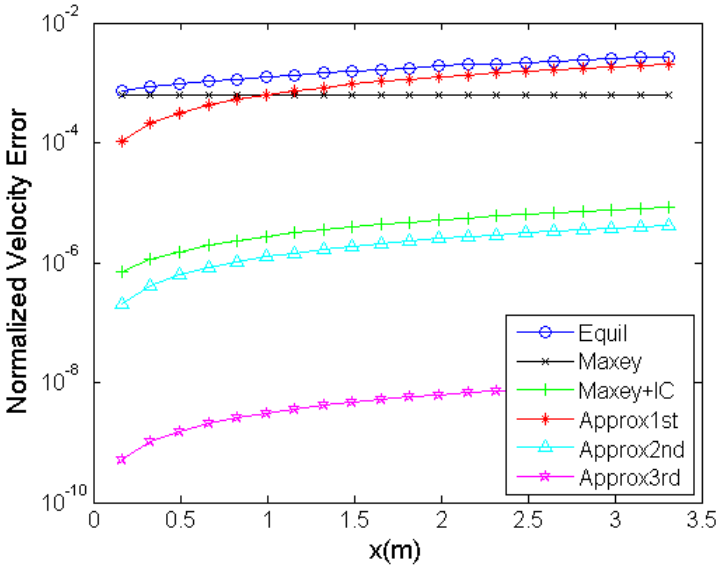

Figure 3.5: Performance of the approximate solutions for $4U_x^o\tau_p = 3.99\text{x}10^{-3}$. Parameters are: $U_x^o = 0.1s^{-1}$, $U^o - V^o = 0.10$ m/s, $t = 1.0$ s, $\tau_p = 1.0\text{x}10^{-2}$s, $U_o = 0.0$ m/s, and $U_t^o = 0.0$ m/s^2

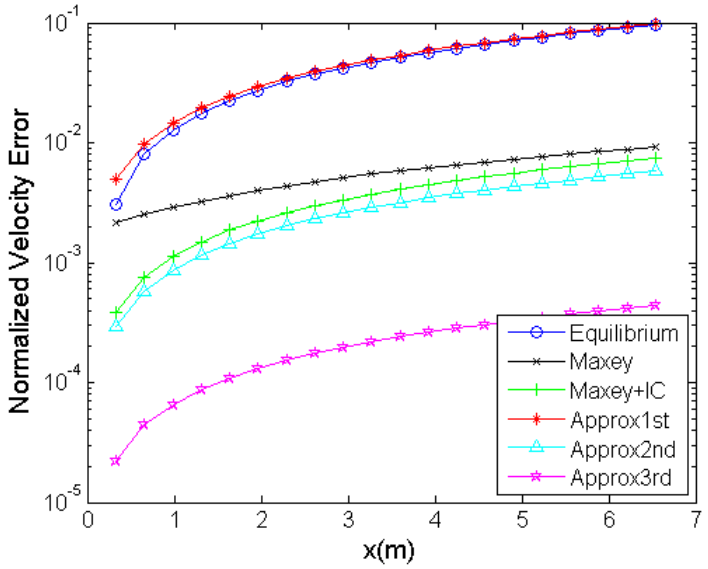

Figure 3.6: Performance of the approximate solutions for $4U_x^o\tau_p = 0.122$. Parameters are: $U_x^o = 1.0s^{-1}$, $U^o - V^o = -0.10$ m/s, $t = 0.8$ s, $\tau_p = 3.1\text{x}10^{-2}$s, $U_o = 0.0$ m/s, and $U_t^o = 0.0$ m/s^2

Varying the droplet time constant and the background velocity gradient while keeping the Stokes number fixed produces the same results. Compare Figure 3.7 below with Figure 3.5.

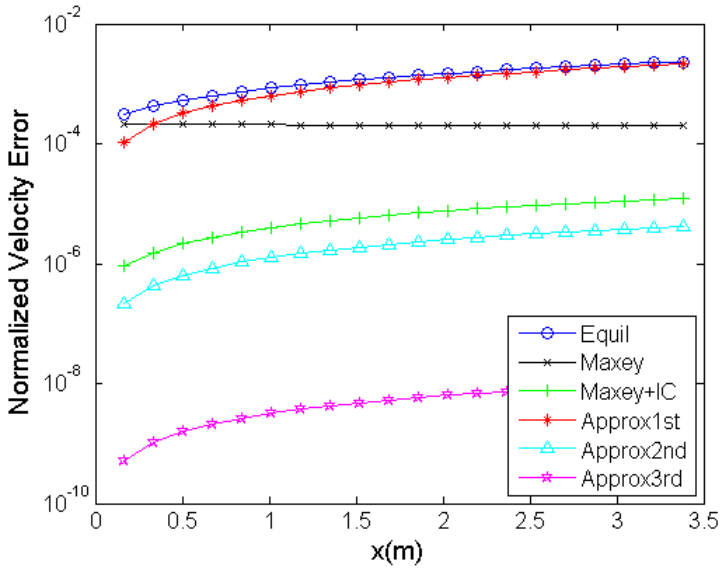

Figure 3.7: Performance of the approximate solutions for $4U_x^o\tau_p = 3.99\text{x}10^{-3}$. Parameters are: $U_x^o = 0.3s^{-1}$, $U^o - V^o = 0.10$ m/s, $t = 0.4$ s, $\tau_p = 3.99\text{x}10^{-3}$s, $U_o = 0.0$ m/s, and $U_t^o = 0.0$ m/s^2

3.3.4 Temporal Departures

The relative size of the spatial variation in the flowfield relative to the temporal variation also plays a critical role in the error schemes. If the temporal changes in the background flow are much larger than the spatial variations (i.e. $U_t^o dt > U_x^o dx$), then the flow is dominated by the particular solution, and the exponential coefficients that are proportional to U_t. Although the solutions do not permit $U_x = 0$, the temporal departures can be isolated by setting $U_x = \epsilon$, a very small quantity.

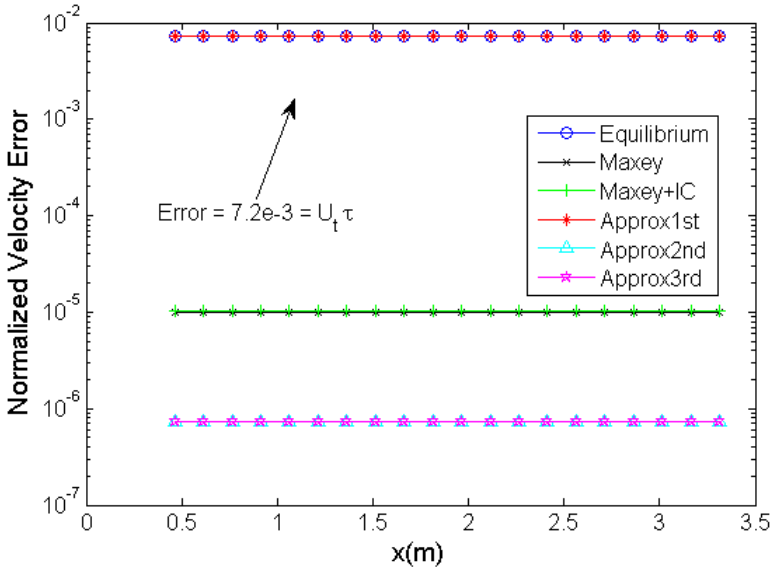

Figure 3.8: Performance of the approximate solutions for $4U_x^o\tau_p = 3.05\text{x}10^{-6}$. Parameters are: $U_x^o = 1.0\text{x}10^{-4}s^{-1}$, $U^o - V^o = 0.10$ m/s, $t = 0.8$ s, $\tau_p = 7.63\text{x}10^{-3}$s, $U_o = 0.0$ m/s, $U_t^o = 1.0$ m/s^2, and $U_t\tau_p = 7.2\text{x}10^{-3}$ (normalized)

.

In a temporally dominated flow all of the particles see essentially the same flowfield so there is no variation in error across the domain. The equilibrium and first order solutions converge to the same error, as supported by the limit equations in section 3.3. The expected second and third order solution convergence is seen as well.

3.3.5 Discussion

This one dimensional case illustrates four essential modes of deviation from equilibrium. The first occurs through finite slip velocities which the equilibrium model does not capture. The slip velocities have transient and lasting effects in the flowfield, as initial error is propagated through time in the trajectory. The magnitude of the velocity deviation due purely to temporal scales is defined by $U_t\tau_p$. The Stokes number represents the third mode of deviation and is governed

by the size of the spatial gradient and the particle timescale. For larger Stokes numbers, a full solution particle cannot follow the fast changes in the flowfield, and exponential growth in equilibrium error is seen. A fourth mode that is not illustrated in the simulations above can occur if the temporal scales $U_t\tau_p$ compete with the advection scale U_oU_x. This particular mode will be explored later in more dimensions. If the spatial and temporal gradients are of the same scale, a combination of these two modes must be accounted for in order to predict equilibrium behavior.

3.4 Special Case: 3D Irrotational Flow

An irrotational flow field presents the opportunity to employ the one dimensional equations derived in the previous sections in fully three dimensional cases, with only slight modifications. The coupled three dimensional equation of motion, Eq. (2.9), can be written in index notation as

$$\frac{d^2}{dt^2}\Delta x_{p,i} + \frac{1}{\tau_p}\frac{d}{dt}\Delta x_{p,i} = g_i + \frac{1}{\tau_p}\left[U_i^o + \frac{\partial U_i^o}{\partial x_j}\cdot\Delta x_{p,j} + \frac{dU_i^o}{dt}t\right]. \tag{3.44}$$

The system is coupled through the presence of $(\partial U_i^o/\partial x_j)\,\Delta x_{d,j}$. Even though standard ODE theory will solve the problem (see next section), the coupling between the equations produces a convoluted expression that does not lend itself to straightforward analysis. In an irrotational case though, the equations can be decoupled. For an irrotational flow we can write

$$\nabla \boldsymbol{U} = \boldsymbol{S} = \sum_{i=1}^{3}\Lambda_i \boldsymbol{a}_i \otimes \boldsymbol{a}_i, \tag{3.45}$$

where $\boldsymbol{a}_i \otimes \boldsymbol{a}_i$ is an orthogonal eigenbasis for the velocity gradient tensor. Substituting (3.45) into (2.9) gives

$$\begin{aligned}\frac{d^2}{dt^2}\Delta \boldsymbol{x}_p + \frac{1}{\tau_p}\frac{d}{dt}\Delta \boldsymbol{x}_p = \boldsymbol{g} + \frac{1}{\tau_p}\left[\boldsymbol{U}(\boldsymbol{x}_p(0),0) + \frac{d\boldsymbol{U}(\boldsymbol{x}_p(0),0)}{dt}t\right] + \\ \frac{1}{\tau_p}\left[\sum_{i=1}^{3}\Lambda_i \boldsymbol{a}_i \otimes \boldsymbol{a}_i \cdot \left(\sum_{\alpha=1}^{3}\Delta x_{p,\alpha}\boldsymbol{a}_\alpha\right)\right].\end{aligned} \tag{3.46}$$

Here, α is used to indicate components of Δx_p in the eigenbasis corresponding to the velocity gradient tensor. Using the definition of the dyadic product ($(\boldsymbol{e}_m \otimes \boldsymbol{e}_n)\cdot\boldsymbol{e}_j = (\boldsymbol{e}_j\cdot\boldsymbol{e}_n)\boldsymbol{e}_m$) and expanding the double sum yields

$$\begin{aligned}\frac{d^2}{dt^2}\Delta \boldsymbol{x}_p + \frac{1}{\tau_p}\frac{d}{dt}\Delta \boldsymbol{x}_p = \boldsymbol{g} + \\ \frac{1}{\tau_p}\left[\boldsymbol{U}^o + \frac{d\boldsymbol{U}^o}{dt}t + \sum_{i=1}^{3}\Lambda_i \boldsymbol{a}_i \delta_{i\alpha}\sum_{\alpha=1}^{3}\Delta x_{p,\alpha}\right].\end{aligned} \tag{3.47}$$

Now, the inner product with $\boldsymbol{a}_\alpha$ is taken, resulting in three uncoupled ODE's, one along each

eigenvector:

$$\left(\frac{d^2}{dt^2}+\frac{1}{\tau_p}\frac{d}{dt}\right)\Delta x_{p,\alpha}=g_\alpha+\frac{1}{\tau_p}\left[U_\alpha^o+\frac{dU_\alpha^o}{dt}t+\Lambda_\alpha\Delta x_{p,\alpha}\right]. \tag{3.48}$$

Equation (3.48) has the same form as the 1D flow field Eq. (3.21), and can be evaluated using the same set of approximate solutions defined in Section 3.3 by substituting Λ_i for U_x and $a_i \cdot \frac{dU_i^o}{dt}$ for U_t. The same conclusions hold as in the 1D case. The flow of heavy particles through weakly rotational flow fields can thus be described using the hierarchy of solutions.

Chapter 4

General Case Solution

The three dimensional equation of motion (2.9) is a system of second order linear ordinary differential equations with constant coefficients. The solution to the system is most easily understood by writing the equations in state space form using a Cartesian basis,

$$\begin{bmatrix} \dot{\Delta x_p} \\ \dot{\Delta y_p} \\ \dot{\Delta z_p} \\ \ddot{\Delta x_p} \\ \ddot{\Delta y_p} \\ \ddot{\Delta z_p} \end{bmatrix} = \begin{bmatrix} 0 & 0 & 0 & 1 & 0 & 0 \\ 0 & 0 & 0 & 0 & 1 & 0 \\ 0 & 0 & 0 & 0 & 0 & 1 \\ & & & & & \\ U_x/\tau_p & U_y/\tau_p & U_z/\tau_p & \frac{-1}{\tau_p} & 0 & 0 \\ V_x/\tau_p & V_y/\tau_p & V_z/\tau_p & 0 & \frac{-1}{\tau_p} & 0 \\ W_x/\tau_p & W_y/\tau_p & W_z/\tau_p & 0 & 0 & \frac{-1}{\tau_p} \end{bmatrix} \begin{bmatrix} \Delta x_p \\ \Delta y_p \\ \Delta z_p \\ \dot{\Delta x_p} \\ \dot{\Delta y_p} \\ \dot{\Delta z_p} \end{bmatrix} + \begin{bmatrix} 0 \\ 0 \\ 0 \\ U_t \Delta t + U^o + \boldsymbol{g} \cdot \hat{i} \\ V_t \Delta t + V^o + \boldsymbol{g} \cdot \hat{j} \\ W_t \Delta t + W^o + \boldsymbol{g} \cdot \hat{k} \end{bmatrix}. \quad (4.1)$$

The general form of the full solution is

$$\Delta \boldsymbol{x}_p = \sum_{i=1}^{6} C_i \boldsymbol{\eta}_i e^{\lambda_i t} + \Delta \boldsymbol{x}_p(t)_{\text{particular}}. \quad (4.2)$$

where $\boldsymbol{\lambda}$ and $\boldsymbol{\eta}$ are the eigenvalues and eigenvectors of the full solution state space matrix. The C_i's are constant scalars.

The governing equilibrium Eq. (2.10) is written in state space form as

$$\begin{bmatrix} \dot{\Delta x_p^{eq}} \\ \dot{\Delta y_p^{eq}} \\ \dot{\Delta z_p^{eq}} \end{bmatrix} = \begin{bmatrix} U_x & U_y & U_z \\ V_x & V_y & V_z \\ W_x & W_y & W_z \end{bmatrix} \begin{bmatrix} \Delta x_p^{eq} \\ \Delta y_p^{eq} \\ \Delta z_p^{eq} \end{bmatrix} + \begin{bmatrix} U_t \Delta t + U^o + \boldsymbol{g} \cdot \hat{i} \\ V_t \Delta t + V^o + \boldsymbol{g} \cdot \hat{j} \\ W_t \Delta t + W^o + \boldsymbol{g} \cdot \hat{k} \end{bmatrix}. \quad (4.3)$$

The equilibrium state space matrix is the velocity gradient tensor, which has eigenvalues that

are referred to as $\mathbf{\Lambda}$. The equilibrium solution, denoted $\Delta \boldsymbol{x}_p^{eq}$ is given by

$$\Delta \boldsymbol{x}_p^{eq} = \sum_{i=1}^{3} C_i^{eq} \boldsymbol{\eta}_i^{eq} e^{\Lambda_i t} + \Delta \boldsymbol{x}_p^{eq}(t)_{\text{particular}}. \tag{4.4}$$

The particular solution corresponds to the inhomogeneous part of the state space system, and for both systems is a linear polynomial in time

$$\Delta \boldsymbol{x}_p(t)_{\text{particular}} = \boldsymbol{r}t + \boldsymbol{s}. \tag{4.5}$$

This form of the particular solution is inserted into the original system in order to solve for the components of the coefficient vectors $\boldsymbol{r}$ and $\boldsymbol{s}$. Notice though, that when the particular solution is inserted into Eq. (2.9) to solve for its explicit form, the second order term vanishes

$$\frac{d^2}{dt^2}\left(\Delta \boldsymbol{x}_p(t)_{\text{particular}}\right) = 0. \tag{4.6}$$

Thus, the particular solution for the equilibrium system and the full system are exactly the same, which was also observed in the one dimensional situation above. The particular solution only affects deviations from equilibrium through the constants, i.e. not the functional form. These effects are secondary and are addressed later. For now, the homogeneous portion of the solution is examined.

From Eq.'s (4.2) and (4.4), it is evident that the behavior of the full system is governed by the eigenvalues λ_{1-6} and the equilibrium system by the eigenvalues Λ_{1-3}. A key expression derived in this work (see Appendix C) is that the relationship between these two sets of eigenvalues is given by

$$\lambda_{1-6} = \frac{-1 \pm \sqrt{1 + 4\Lambda_{1-3}\tau_p}}{2\tau_p}. \tag{4.7}$$

Again, Λ_{1-3} are not only the eigenvalues of the equilibrium state space matrix but also of the velocity gradient tensor. Analogous to the system in 1D, a hierarchy of solutions can be derived based on the expansion of $\sqrt{1 + 4\Lambda_{1-3}\tau_p}$, where $4\Lambda_{1-3}\tau_p$ are the small parameters. In the limit of small $\Lambda_{1-3}\tau_p$ (with $\Lambda_{1-3}\tau_p \neq 0$), all hierarchical solutions converge to the first-order or linear expansion. In this limit, the relationship between the full system eigenvalues and the equilibrium system is

$$\lambda_{1,3,5} = \Lambda_{1,2,3} \quad \text{and} \quad \lambda_{2,4,6} = -1/\tau_p - \Lambda_{1,2,3}. \tag{4.8}$$

Full system eigenvalues $\lambda_{2,4,6}$ correspond to the transient portion of the droplet motion and are expected to decay to zero beyond $\sim 3\tau_p$. Hence, the remaining portion of the full solution, which is controlled by $\lambda_{1,3,5}$, becomes equal to the general form of the equilibrium solution as shown in Eq. (4.8). Thus, analogous to the situation in 1D, in the limit as $\Lambda_{1-3}\tau_p$ approaches zero, the general form of the full solution converges to the equilibrium form. The discriminating parameter is $\Lambda_{1-3}\tau_p$. The maximum entry of this vector is the natural choice for a Stokes number

since it governs the largest deviations from equilibrium through time.

$$\boxed{St = \mathrm{Max}(\Lambda_{1-3}\tau_p)} \tag{4.9}$$

The Stokes number is the most critical parameter in determining deviations from equilibrium but does not account for temporal variations in the flow field. In steady situations, it is easy to show that the slip velocity and the Stokes number are sufficient criteria for predicting equilibrium. This is done in Chapter 5.

In unsteady cases, temporal error effects arise through the solution constants C_i and C_i^{eq}. The impact of these temporal terms is secondary to the spatial effects, which govern the exponential behavior. The temporal effects do have an important role in the size of the exponential coefficient, and are the governing source of error if the spatial gradients are insignificant. This interplay between $\boldsymbol{U_t^o}$ and Λ will be demonstrated numerically in Chapter 6.

Chapter 5

Stuart Vortex Demonstration

To illustrate droplet motion in a meaningful flow, the Stuart vortex is employed [22]. The Stuart vortex is an exact solution of the steady planar Euler equations, and is a model for planar vortices [25]. The particular form used here is defined by

$$U_1(x,y) = -U_\infty \frac{\sinh(2\pi y/\alpha)}{\cosh(2\pi y/\alpha) - k\cos(2\pi x/\alpha)} \text{ (horizontal velocity)} \tag{5.1}$$

$$U_2(x,y) = U_\infty k \frac{\sinh(2\pi x/\alpha)}{\cosh(2\pi y/\alpha) - k\cos(2\pi x/\alpha)} \text{ (vertical velocity).} \tag{5.2}$$

Here α is related to the spatial frequency of the vortices while U_∞ and k govern the magnitude of the velocity. A sample Stuart vortex vector field is plotted in Figure 5.1.

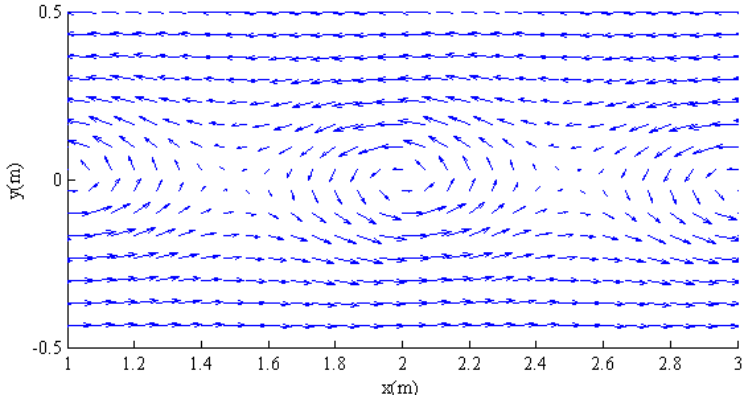

Figure 5.1: Stuart vortex velocity field for $\alpha = 0.25$m, $U_\infty = 13.43$ m/s and $k = 0.5$.

Two sets of droplets were placed into this flowfield and advected; one with the full EoM and the other with the equilibrium EoM. Since there is no gravity in this problem, equilibrium effectively amounts to passive scalar advection. Two thousand droplets were given zero initial

slip velocity and a uniform initial distribution as shown in Figure 5.2. Table 5.1 provides the parameters used in these simulations.

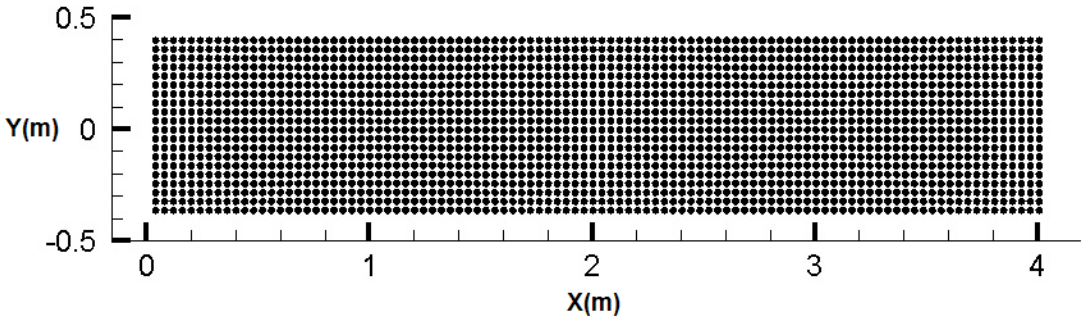

Figure 5.2: Initial distribution of particles in the Stuart vortex (2000 total).

ρ_p (kg/m^3)	μ_f (Ns/m^2)	k (rad)	α (m)	r_p (m)	U_∞ (m/s)
5000 (light metal)	1.5e-5 (air)	0.5	0.25	Varies	Varies

Table 5.1: Parameters for the Stuart vortex simulations

The purpose of these simulations is to show that the $\Lambda\tau_p$ Stokes number is an effective predictor of equilibrium behavior. The Stuart vortex, being a steady flow field, provides the opportunity to do this without considering the interaction between temporal and spatial influences. Contour plots of the flow field are constructed using the parameter $4 * \tau_p * \text{Max}(|\Lambda_i|)$ (the norm is necessary to account for complex eigenvalues). In this flow field, the droplets advected using the equilibrium EoM are plotted in yellow, and then the droplets advected using the full EoM are plotted over top in black. If the equilibrium state is an adequate description of the dynamics then the solution will not display any yellow droplets.

Figure 5.3 depicts three simulations in order of decreasing $4\tau_p\text{max}(|\Lambda|)$ in the flowfield. Figure 5.3(a) is an example of a flow in which the equilibrium condition is not prominent. Comparing the full solution to the equilibrium solution, the only regions where the solutions match are far away from the vortices. The strong vortex, coupled with a sufficiently large τ_p, forces the droplet field out of the equilibrium state. In Figure 5.3(b), the maximum value of the Stokes number, has been roughly halved. The two sets of points match well for most of the flow, except in the interior regions of the vortex as before. Figure 5.3(c) depicts a situation where $\Lambda_{1-3}\tau_p$ is small. There is almost no difference between the full solutions and the equilibrium solution throughout the flow field. Note that in all of these simulations, the quantity U_∞ multiplied by the advection time has been fixed to 0.2 m, so that particles travel approximately the same distance between simulations.

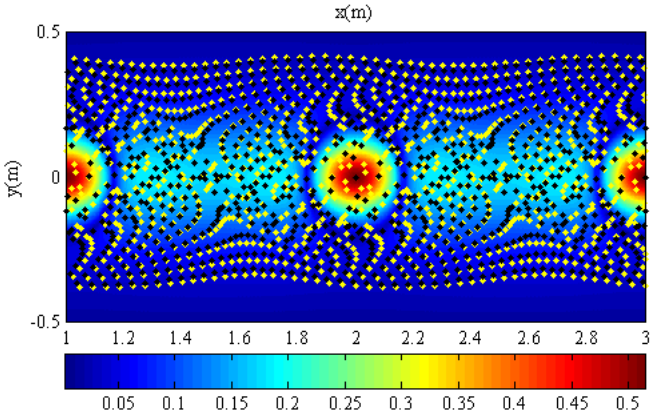

(a) Maximum $4\tau_p \max(|\Lambda|) = 0.516$. $U_\infty = 4$m/s and $r_d = 7.0$ microns at $t = 0.2$s.

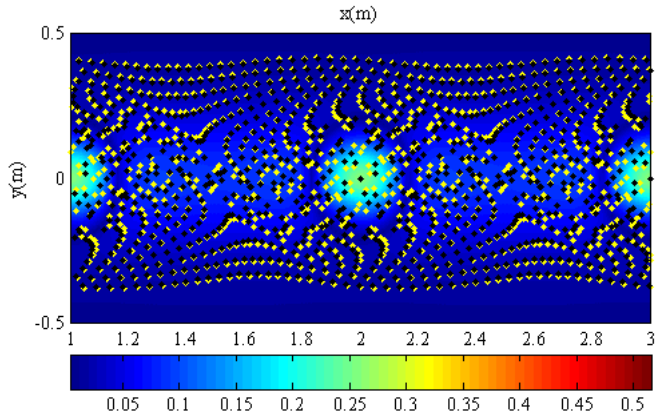

(b) Maximum $4\tau_p \max(|\Lambda|) = 0.258$. $U_\infty = 8$m/s and $r_d = 3.5$ microns at $t = 0.1$s.

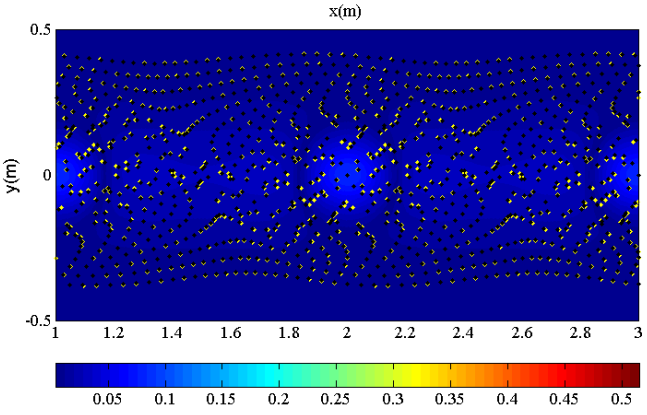

(c) Maximum $4\tau_p \max(|\Lambda|) = 0.084$. $U_\infty = 2$m/s and $r_d = 4$ microns at $t = 0.4$s.

Figure 5.3: Stuart Vortex fields with increasing values of $4\tau_p \max(|\Lambda|)$ plotted in contour. Equilibrium droplets are yellow and full solution droplets are black.

Initial slip velocity can also have a pronounced effect on the equilibrium discrepancy. Slip velocity is introduced as a random bounded percentage that multiplies the initial background velocity. It takes very large slip velocities to introduce noticeable discrepancies from zero slip behavior over times that are much greater than $3\tau_p$. Figure 5.4(a) contains the same conditions as figure 5.4(b), but includes a random initial velocity that is 50 to 200% of the original background velocity. Despite this extreme initial slip condition, the average positional error only increases by 19%, and this additional error only accounts for 0.07% of the average total traveling distance. This is an isolated case though, where high accuracy is expected. The intensity of slip velocity errors heavily depends on size of τ_p, the advection time, and the strength of the spatial gradients, which propagate and magnify small velocity differences.

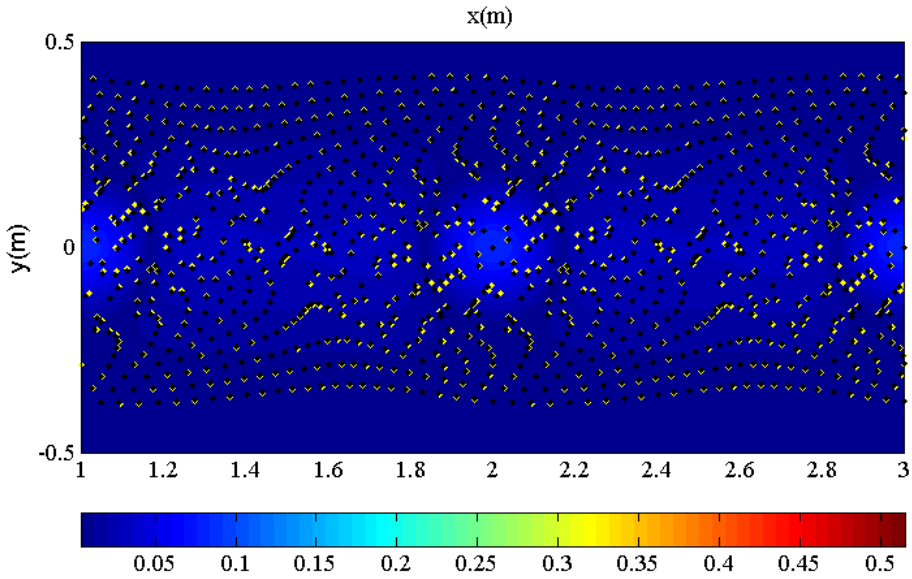

(a) Maximum $4\tau_p \max(|\Lambda|) = 0.084$. $U_\infty = 2$m/s and $r_d = 4$ microns at $t = 0.4$s. Average positional error: 0.0030 m

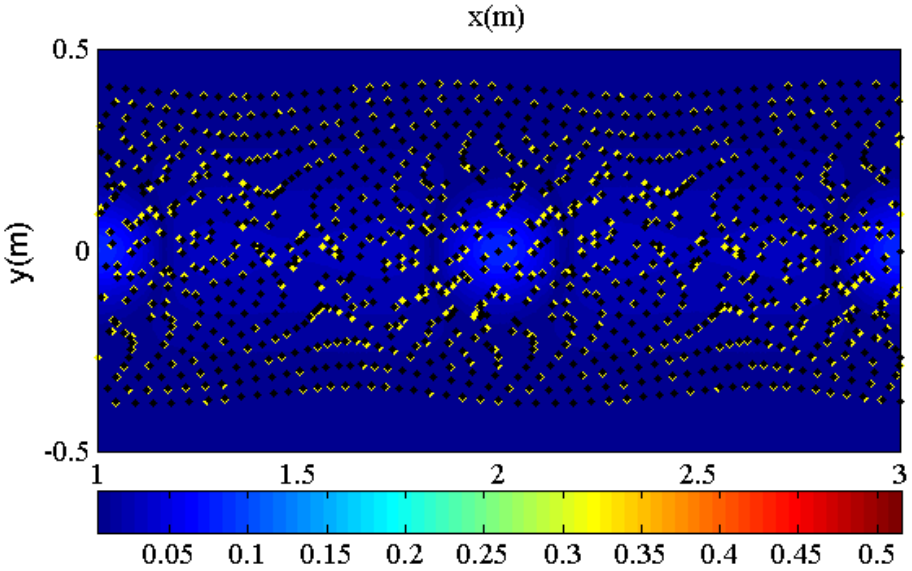

(b) Contour plot of $4\tau_p \max(|\Lambda|)$ field for Stuart Vortex with $U_\infty = 2$m/s and $r_d = 4$ microns at $t = 0.4$s. Maximum $4\tau_p \max(|\Lambda|) = 0.084$. Equilibrium droplets are yellow and full solution droplets are black. Slip velocity varies from 50-200% of background flow velocity. Average positional error: 0.0036 m

Figure 5.4: Initial slip velocity shows a pronounced effect in (b). Equilibrium droplets are yellow and full solution droplets are black.

In order to demonstrate that the Stokes number is a proper governing parameter for equilibrium, as opposed to only considering τ_p or Λ, the simulation is carried out holding $\Lambda\tau_p$ constant, but varying Λ and τ_p individually. The result of this exercise is shown in Figure 5.5(a), which has the same $\Lambda\tau_p$ characteristic as in Figure 5.5(b), but with different Λ and τ_p parameters. Varying Λ and τ_p individually while keeping $\Lambda\tau_p$ constant produces the same error behavior between solutions; thus confirming that the key non-dimensional quantity controlling the departure is $\Lambda\tau_p$.

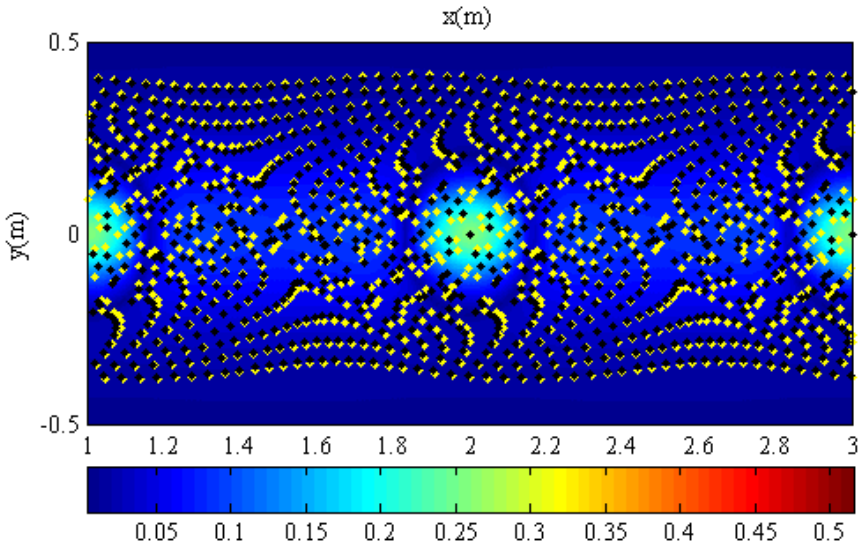

(a) Maximum $4\tau_p \max(|\Lambda|) = 0.258$. $U_\infty = 8$m/s and $r_d = 3.5$ microns at $t = 0.1$s.

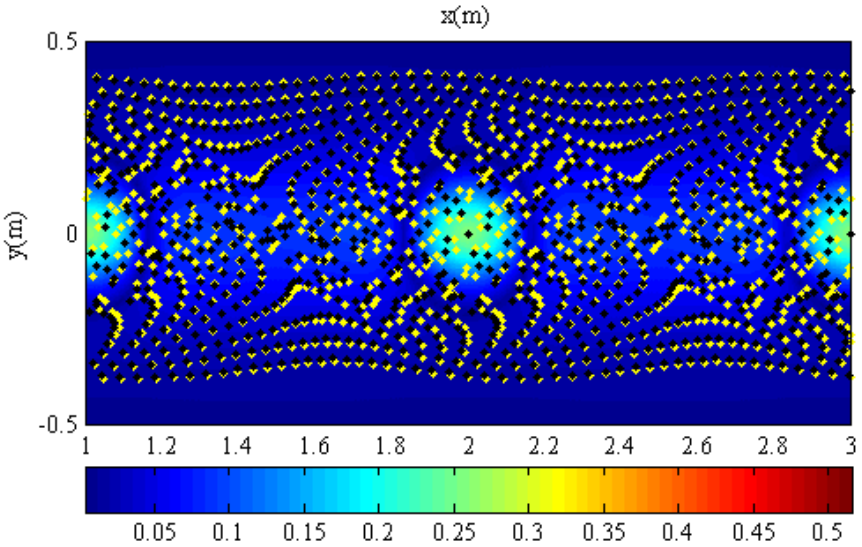

(b) Maximum $4\tau_p \max(|\Lambda|) = 0.258$. $U_\infty = 2$m/s and $r_d = 7$ microns at $t = 0.4$s.

Figure 5.5: Stuart Vortex fields with equal values of $4\tau_p \max(|\Lambda|)$, while varying individual parameters. Equilibrium droplets are yellow and full solution droplets are black.

A natural choice for the traditional Stokes number of the stuart vortex would be $St = \tau_p \frac{U_\infty}{\alpha}$. This disregards conditions in the interior of the vortex, and would not be sufficient to predict equilibrium behavior. Even if the background velocity for the Stokes number was evaluated locally at the particle location, the choice of representative length scale presents difficulty. The conventional Stokes number $\tau_p \frac{U_f}{L_f}$ only approximates $\tau_p \frac{d\boldsymbol{U}}{d\boldsymbol{x}}$,which is effectively represented by the $\Lambda\tau_p$ Stokes number.

Chapter 6

3D Benchmarking Flow Field

The primary parameter governing divergence from equilibrium through time is the heavy particle Stokes number $\Lambda\tau_p$, as shown in Chapter 4. The temporal mechanisms for equilibrium departure are very well understood in the absence of spatial variations, but must also be addressed for realistic flow fields that contain both spatial and temporal variations. The coupling between the spatial scales and the temporal scales in three dimensions cannot explicitly be written due to the algebraic complexity of the constants in Eq. (4.2). The alternative option is to numerically show how the two relate. This is done using a fully analytical solution to the Navier-Stokes solutions owed to Ethier and Steinman [4]. Given spatial coordinates (x, y, z), and two real positive numbers a and b, the benchmarking flow velocity field u, v, w is given by

$$\begin{aligned} u &= -a\left[e^{ax}\sin\left(ay+dz\right)+e^{az}\cos\left(ax+dy\right)\right]e^{-d^2t} \\ v &= -a\left[e^{ay}\sin\left(az+dx\right)+e^{ax}\cos\left(ay+dz\right)\right]e^{-d^2t} \\ w &= -a\left[e^{az}\sin\left(ax+dy\right)+e^{ay}\cos\left(az+dx\right)\right]e^{-d^2t} \end{aligned} \tag{6.1}$$

The only condition imposed on the flow is incompressibility. The flow field is unsteady, and contains nonzero convective, pressure, and diffusion terms. Therefore, it has some account of all physical mechanisms described by the Navier-Stokes equations, and makes no unnecessary simplifications. A visualization of the velocity field that shows how the parameter $\max|\Lambda|$ varies is depicted in figure 6.1.

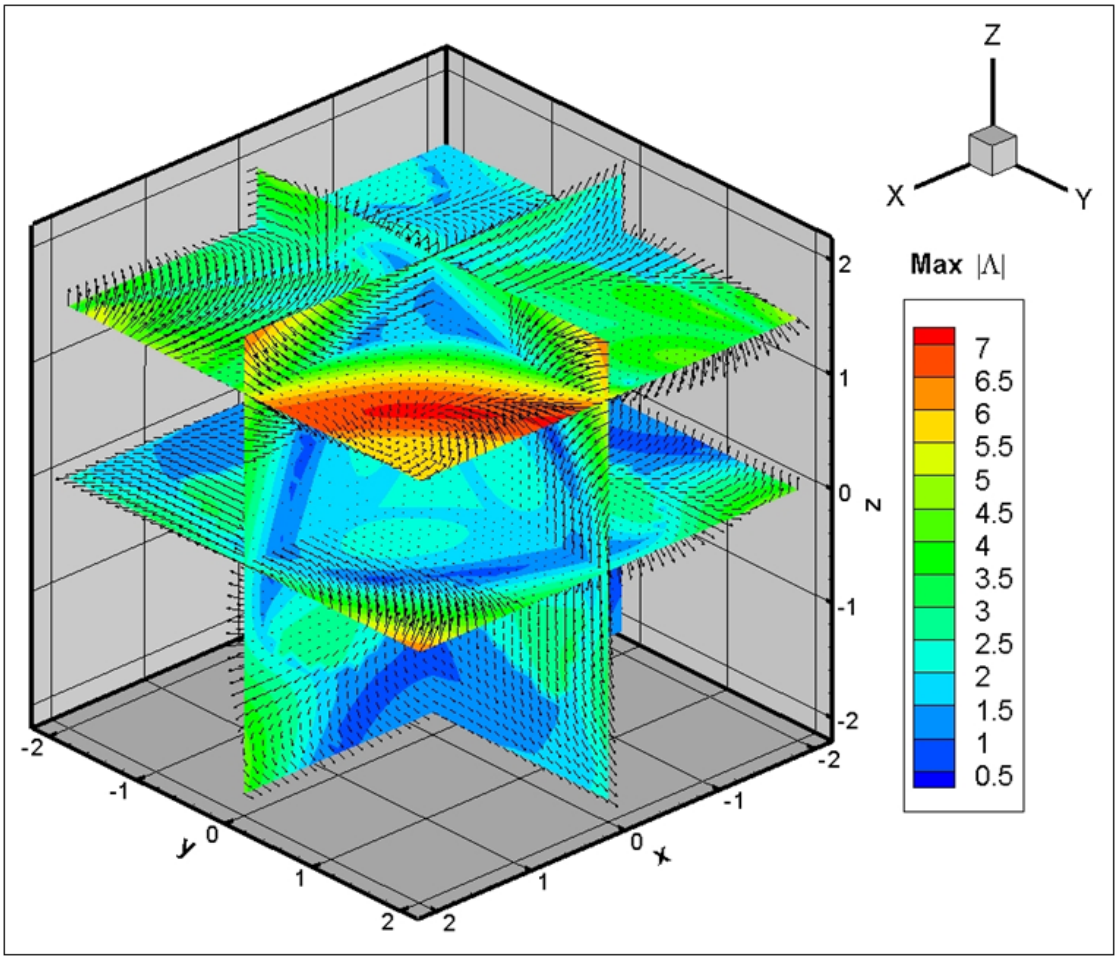

Figure 6.1: Vector plot of benchmarking flow field for $a = \pi/4$, $d = \pi/2$, and $t = 0$. Planes contoured by $\max(|\Lambda_i|)$ reveal spatial variations.

The flow field itself is difficult to visualize. Ethier and Steinman describe it as a "series of counter-rotating vortices intersecting one another at oblique angles".

The benchmarking flow field is much more complex than the Stuart vortex. The three-dimensionality of the flow field makes the simple visual technique that displayed error in the Stuart vortex a poor tool for accurately revealing errors in the benchmarking flow field. Nonetheless, a similar analysis can reveal general behaviors, before looking at a detailed rigorous approach. Particles are seeded in a plane, given zero initial slip velocity, and advected using the full equation of motion and the equilibrium equation of motion. The particle endpoints are compared against contour plots of Max(Λ) in the plane. The advection time is chosen to be short, such that the particles remain within 0.1m of the plane, and the contour plot is a reasonable reflection of the background flow field that the particle sees.

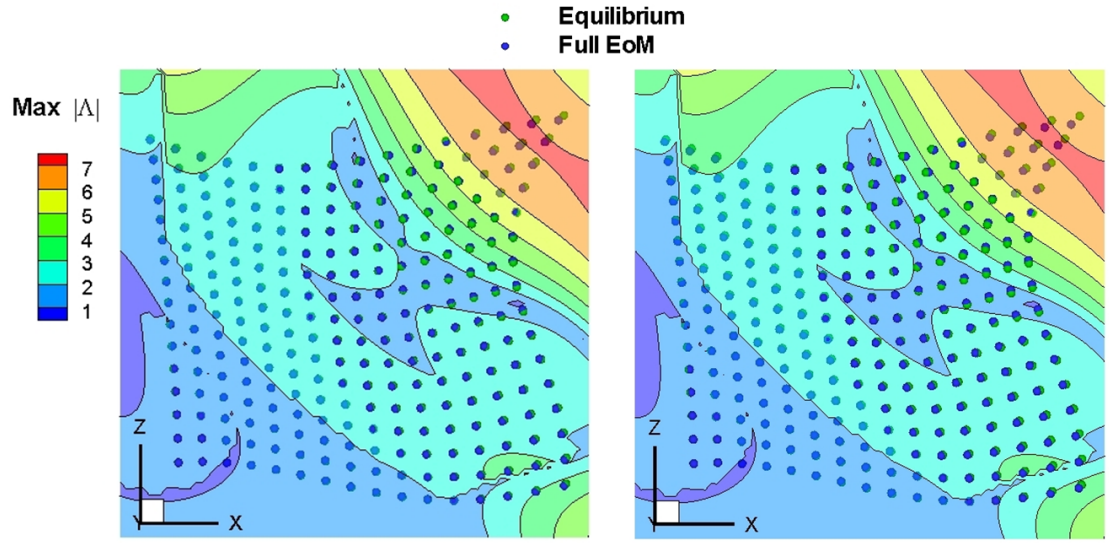

Figure 6.2: Benchmarking flow field simulation with a planar distribution of particles at $y = 0.9$m, with $a = \pi/4$, $d = \pi/2$, and $t = 0.1$s. The left plot particles have $r_p = 20\mu$m, and the mean position error is $0.010m$. The right plot particles have $r_p = 40\mu$m, and the mean position error is 0.018m. Note the correlation between error and particles that have passed through high Λ regions.

The plot on the left uses particles with a 20 micron radius and the plot on the right uses particles with a 40 micron radius. Although the particles do leave the plane and enter different regions, the plots demonstrate a behavior that strongly correlates error with the heavy particle Stokes number $\Lambda\tau_p$.

In the following simulations, a particle is placed in the flowfield, and its trajectory is studied relative to an equilibrium trajectory as a function of the background flow properties, which include $\boldsymbol{U}$, $\nabla\boldsymbol{U}$ and $\boldsymbol{U}_t$. The general case solutions, Eq.'s (4.4) and (4.2), are used to calculate displacement under the full equation of motion and under equilibrium conditions. This requires solving for the general solution initial value problem constants using the zero initial displacement condition, and the zero initial slip velocity. A computationally efficient way to do this in one dimension is given in Appendix A, which is easily modified to give the solution in three dimensions. The validity of the first order Taylor series expansion must also be ensured through the solution time.

Four primary factors appear in the one-dimensional flow field that are involved in a particles divergence from equilibrium. The error difference for x_p^{A2}, equation 3.33, is written here again for simplicity in demonstrating these four factors. Here gravity has been removed since it is not present in the benchmarking flow field.

$$\Delta x_p^{A2} - \Delta x_p^{eq} = \underbrace{\left[\frac{\underbrace{\tau_p\left(V_o - U_o\right)}_{\text{Slip Velocity}} + \underbrace{U_x\tau_p\left(U_o\tau_p\right)}_{\text{Advection}} + \underbrace{U_t\tau_p^2}_{\text{Temporal Accel}}}{1 + 2U_x\tau_p - 2U_x^2\tau_p^2}\right]}_{\text{Exponential}} \underbrace{e^{U_x t - \cancel{\tau_p U_x^2 t}^{0}}}_{\text{Exponential}}$$

$$+ \underbrace{\left[\frac{\tau_p\left(U_o - V_o\right) - U_x\tau_p\left(U_o\tau_p\right) - U_t\tau_p^2}{1 + 2U_x\tau_p - 2U_x^2\tau_p^2}\right] e^{\left(-1/\tau_p - U_x + \tau_p U_x^2\right)t}}_{\text{Transient Terms}} \tag{6.2}$$

How these factors translate to three dimensions is explored by analyzing the trajectory of a single particle under various conditions in the background flow field. These conditions are controlled by varying by varying a and d.

The exponential portion of the behavior is the first factor and is controlled by the $\Lambda\tau_p$ Stokes number, reducing $e^{\lambda t}$ to $e^{\Lambda t}$. The exponential is only a multiplicative coefficient of other terms but it can influence the behavior of the error separately from the other terms as will be shown in the subsequent analysis. In the benchmark flow simulation, this factor will be analyzed by calculating Max($|\Lambda_i|$) for a given particle at its initial location (meaning the maximum of the three $|\Lambda|$'s not the norm of the vector comprising the three). This parameter will be known as the exponential of the spatial gradient. The temporal acceleration U_t is the second factor, and produces a constant linear bias in the coefficient of the exponential. It is accounted for by evaluating $|\{|U_t|, |V_t|, |W_t|\}|$. When weighted by $\tau_p(t + \tau_p)$, this is a representation of the linear temporal contribution to $|\boldsymbol{x}_p^F - \boldsymbol{x}_p^{eq}|$ in the absence of spatial variation.

The advection represented by the U_oU_x term is the third factor. In the benchmarking flow field, this spatial acceleration is directly related to the spatial gradient Λ. In order to preserve this relationship, the advection factor is calculated for particles as max $(\boldsymbol{U} \cdot \boldsymbol{\eta}_i\Lambda_i)$. This calculates the advection term in the eigendirections. This methodology ensures that the effects of off diagonal terms in the velocity gradient matrix are captured. Finite initial slip velocity is the fourth factor. This is expected to remain low in most conditions where particle Reynolds number remains low.

The particle properties are representative of soot in air at STP, with a soot density of $1g/cc^3$ and radius of 10 microns, resulting in a τ_p of 0.0015s. This is kept constant throughout these simulations with the understanding that changing it primarily serves to magnify the effects of the three factors discussed above to different degrees. The simulation end time and position is within $\mathbb{R}^4_{\text{lin}}$, except where noted. The table below shows the $\Delta\boldsymbol{x}$ percentage error between the general solution and standard euler advection (which updates the flowfield as the particle moves) for the most extreme case in each figure. This shows that the $\mathbb{R}^4_{\text{lin}}$ space is an acceptable approximation to the flow field in the simulations to follow.

Figure	6.3	6.4	6.5	6.6	6.6	6.7
End Time	$10\tau_p$	$50\tau_p$	$10\tau_p$	$10\tau_p$	$50\tau_p$	$50\tau_p$
Displacement % error	0.035	.041	0.036	0.21	1.48	1.46

Table 6.1: Validation of the use of $\mathbb{R}^4_{\text{lin}}$ in the figures to follow. Particles are advected using the general solution, and standard euler advection that updates the flowfield along the path. The percentage error above is calculated as the norm of the vector difference between the two displacements, which is then normalized by the standard euler advection displacement distance and multiplied by 100.

The explicit general solutions are used instead of euler advection to show that computation time can be reduced by solving for the local particle displacement explicitly, even if no equilibrium approximation is made. The final error for a particles trajectory is calculated by taking the norm of the vector between the equilibrium particle position and the full EoM particle position.

Although typically the exponential behavior is dominant, for a given flow field it is possible to have any one of the three factors controlling the error. An accurate picture of these scenarios can be obtained by varying the factors a and d. The a parameter primarily controls spatial variations and d primarily controls temporal variations through the e^{ax} terms and trigonometric terms in the benchmark flow field definitions, Eq. (6.1). The equations show that d also influences spatial variations through the sine and cosine terms. Even though the d parameter can influence the spatial gradients, the temporal influence can be isolated reasonably well from the spatial effects by lowering the value of a relative to d. If the spatial gradients are negligible, then the coordinate directions become decoupled. The error in each direction can be calculated independently then according to Section 3.1, and the total error the particle sees can then be calculated as

$$\text{Temporally Dominated Flow Error Prediction} = |\boldsymbol{x}_p^F - \boldsymbol{x}_p^{eq}| = \tag{6.3}$$

$$|\tau_p \left(\boldsymbol{V}^o - \boldsymbol{U}^o\right) \left(1 - e^{-t/\tau_p}\right) - \boldsymbol{U}_t \tau_p t + \tau_p^2 \boldsymbol{U}_t \left(1 - e^{-t/\tau_p}\right)|. \tag{6.4}$$

The situation where this equation is valid, when the spatial gradient exponentials and advection terms are negligible, is referred to as a temporally dominated flow field. The norm of the vector consisting of the error in each direction is taken. Figure 6.3 is a demonstration of this decoupling. It depicts the error through four particles trajectories through time under various values of d and a small value of a. The advection, spatial gradient exponential, temporal acceleration parameters, and analytical error predictions are calculated as above.

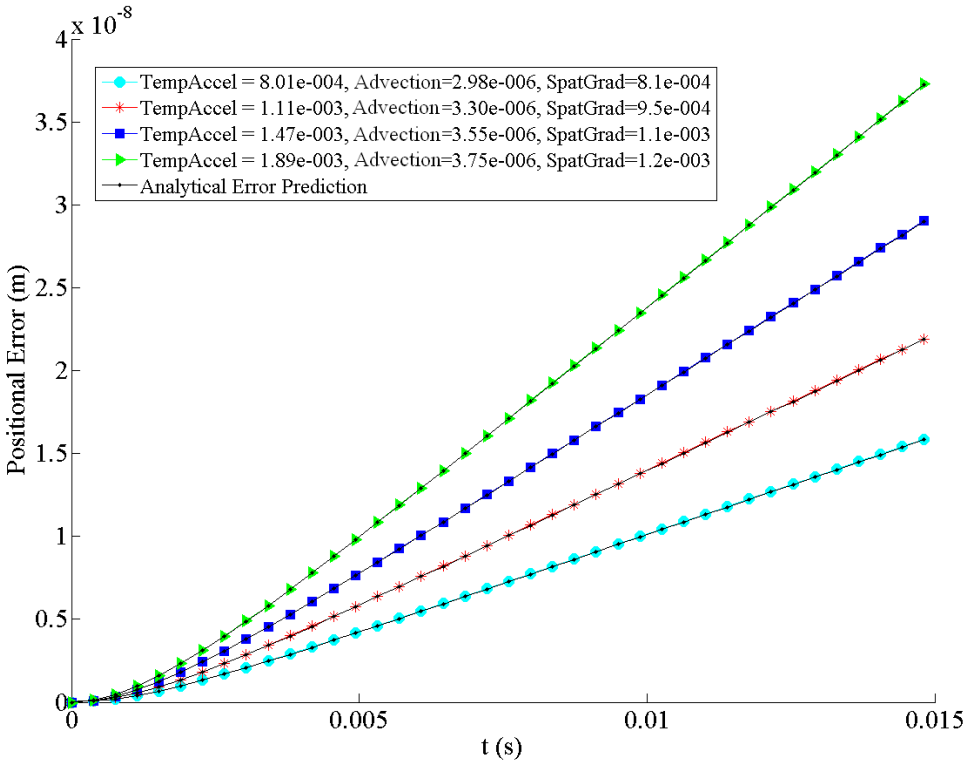

Figure 6.3: Equilibrium error in particle trajectory for various temporally dominated conditions in the benchmarking flow field. Here, $a = \pi/2048$, $d = \pi/6$ through $\pi/4$, $t = 0$ through $10\tau_d \approx 0.015$s, and there is no slip velocity. The linear growth of the error relates to the growth of the temporal accelerations, and not the other parameters. Equation 6.3, which predicts the errors almost exactly, is plotted as a black line. Particle initial position is $(0.90, -0.53, 0.21)$.

Equation (6.3) predicts the error very well, indicating that the flow conditions are dominated by the temporal effects. As a result, the solution decoupled in space and can be expressed by the 1D form showing explicitly the linear behavior of error with time, as well as the initial transient effects. The calculations shown in Figure 6.3 are a numerical confirmation of the linear temporal dependence in the equilibrium departure.

Although the plot above only tracks the particles through $10\tau_p$, it should be noted that the spatial gradients are small enough in this particular scenario that the linear behavior is maintained through $t = 5000\tau_d$, when discrepancies between the purely temporal prediction and the actual error begin to become visible. That length of travel leaves the linear first order Taylor series region for this particular flow field, but it does demonstrate the potential for large computational savings in other flows where $\mathbb{R}^4_{\text{lin}}$ may be larger.

The slip velocity contributions to error in a temporally dominated situation include a decaying term and a constant bias $\tau_p \left(\boldsymbol{V}^o - \boldsymbol{U}^o \right)$. Slip velocity is implemented by forcing the initial velocity to be $\boldsymbol{V}^o = \boldsymbol{U}^o k$, where k is called the slip factor.

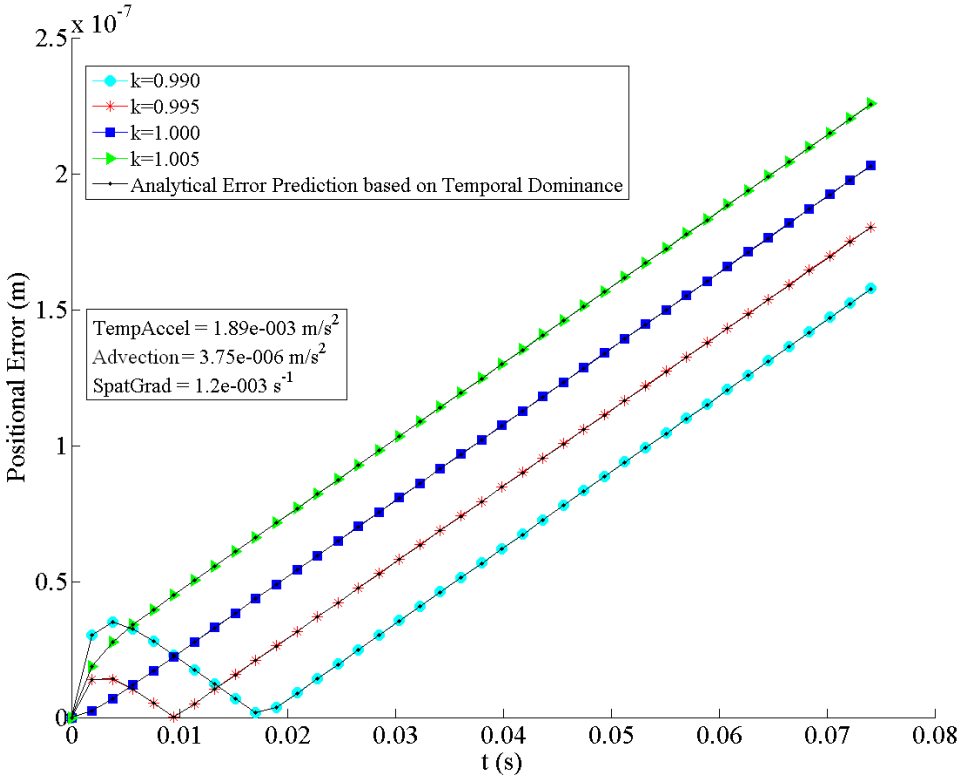

Figure 6.4: Slip velocity in a temporally dominated situation. Here, $a = \pi/2048$, $d = \pi/4$, $t = 0$ through $50\tau_p \approx 0.015$s, and $k = 0.99$ through 1.005. In this flowfield $\boldsymbol{U}^o$ is entirely negative, and $\boldsymbol{U}_t$ entirely positive. Particle initial position is $(0.90, -0.53, 0.21)$.

The hills in the graph above arise because so that the forced particle velocity is artificially low relative to its eventual bias. The flowfield $\boldsymbol{U}^o$ is entirely negative in this flowfield, and $\boldsymbol{U}_t$ is entirely positive, so that this behavior corresponds to particles having $k < 1$, according to Eq. 6.3. The velocity of the particle "catches up" to what its eventual bias must be, and passes through the equilibrium point along its way. After the transient effects are resolved, the error difference in a temporally dominated flow between a particle with arbitrary k and a particle with no slip velocity is $|\tau_p \boldsymbol{U}^o (k-1)|$.

It does not take large advection terms or spatial gradients to introduce errors into the purely temporal approximation though, as demonstrated in Figure 6.5 below.

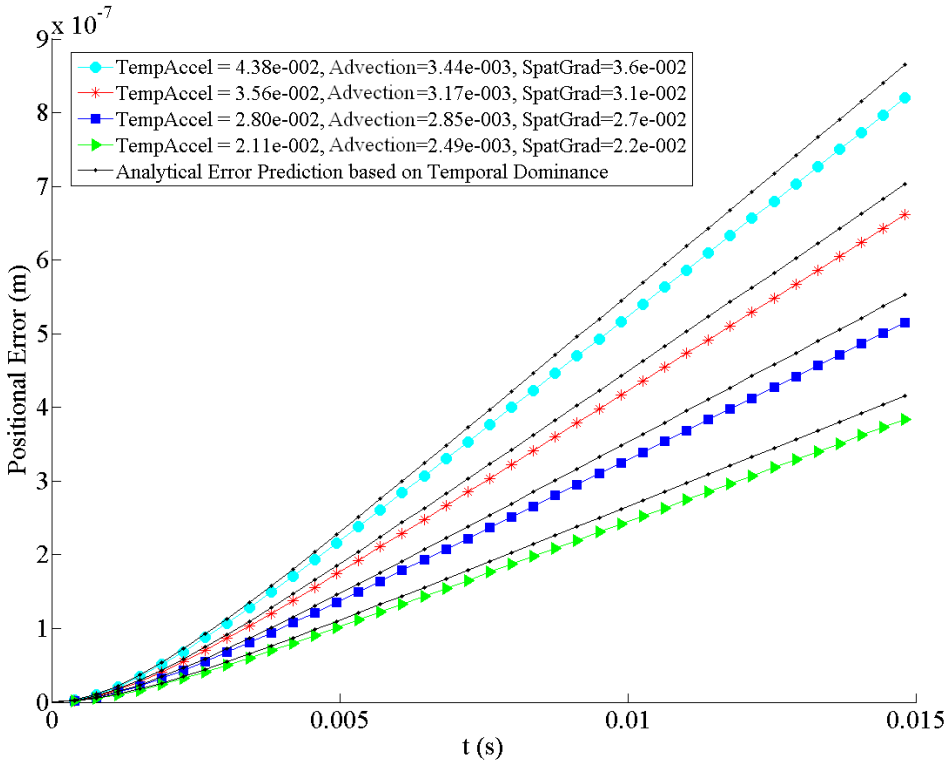

Figure 6.5: Introduction of spatial factors into benchmark flowfield simulation. Here, $a = \pi/64$, $d = -\pi/4$ through -$\pi/6$, and $t = 0$ through $10\tau_p \approx 0.015$s. The growth of the error is due to advection terms, and the exponential influence of the spatial gradients is not a factor. Particle initial position is $(0.90, -0.53, 0.21)$.

The spatial gradients above are very small so that the exponential approximation bringing λ to Λ is valid. The exponential influence then is to scale the error by approximately $e^{\mathrm{Max}(|\Lambda_i|)t}$. Evaluating this quantity for the highest simulation time and largest $e^{\mathrm{Max}(|\Lambda_i|)t}$ gives $e^{(3.6e-2)*0.015} = 1.0005$ and shows that the exponential influence is insignificant. The errors above are directly related to the interplay between the temporal accelerations and finite advection. Predicting this error correctly requires solving completely for the solution constants in the general solution in Chapter 4. This is not attempted in this work, however a few important features can be noted. It has been observed that as long as $e^{\mathrm{Max}(|\Lambda_i|)t}$ remains insignificant, the error with significant advection remains linear. This behavior should be expected because the Maclaurin series for the exponential function,

$$e^{\Lambda t} = 1 + \Lambda t + \frac{(\Lambda t)^2}{2!} + \frac{(\Lambda t)^3}{3!} \cdots \tag{6.5}$$

causes a linear growth in time of the corresponding coefficient of $e^{\Lambda t}$ for small Λt. The usefulness of this observation depends on the flow field in question. In this particular instance, the error

remains visibly linear in time until $t = 2000\tau_d \approx 3s$, when $e^{3.6e-2*3} = 1.11$.

When the spatial gradients are significant, the error exhibits exponential growth. This situation is depicted in Figure 6.6 below.

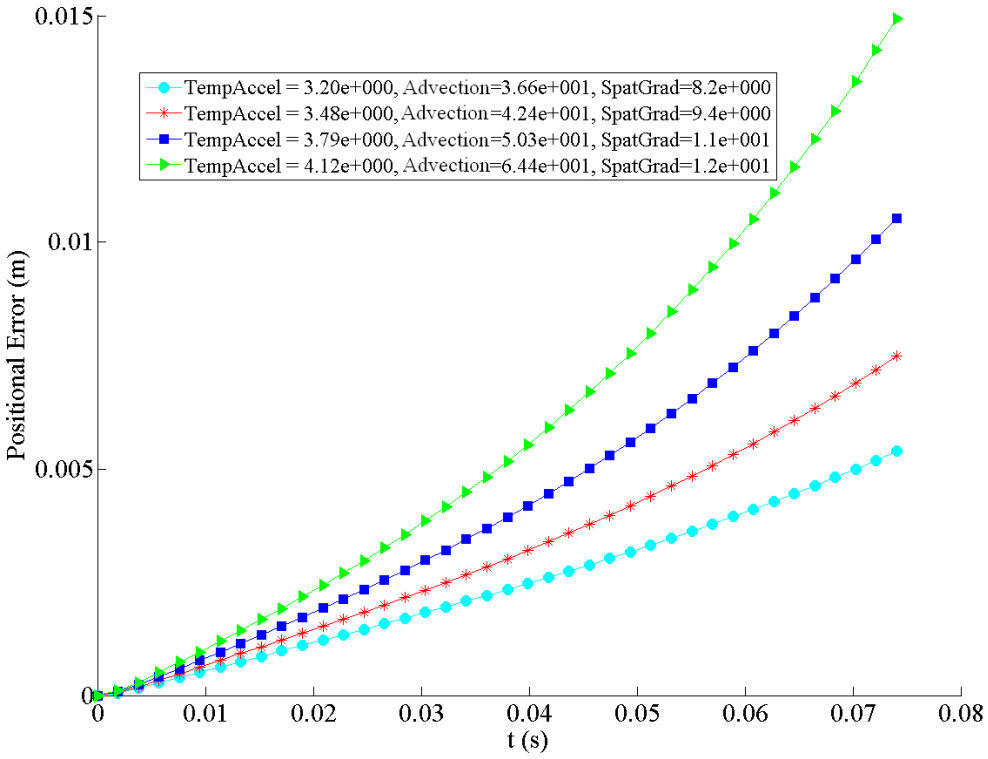

Figure 6.6: Benchmarking flow varying the a parameter showing exponential influence. Here, $a = \pi/2.25$ through $\pi/2$, $d = \pi/4$, and $t = 0$ through $50\tau_d \approx 0.075s$. Particle initial position is $(0.90, -0.53, 0.21)$.

The error behavior through a trajectory is very sensitive to the spatial gradient parameter. Note that the discrepancy in using $\mathbb{R}^4_{\text{lin}}$ has been pushed to 1.48% here to show the exponential quality of the particles trajectory errors. Figure 6.7 depicts the result of introducing finite slip velocities into a flow with significant spatial gradients.

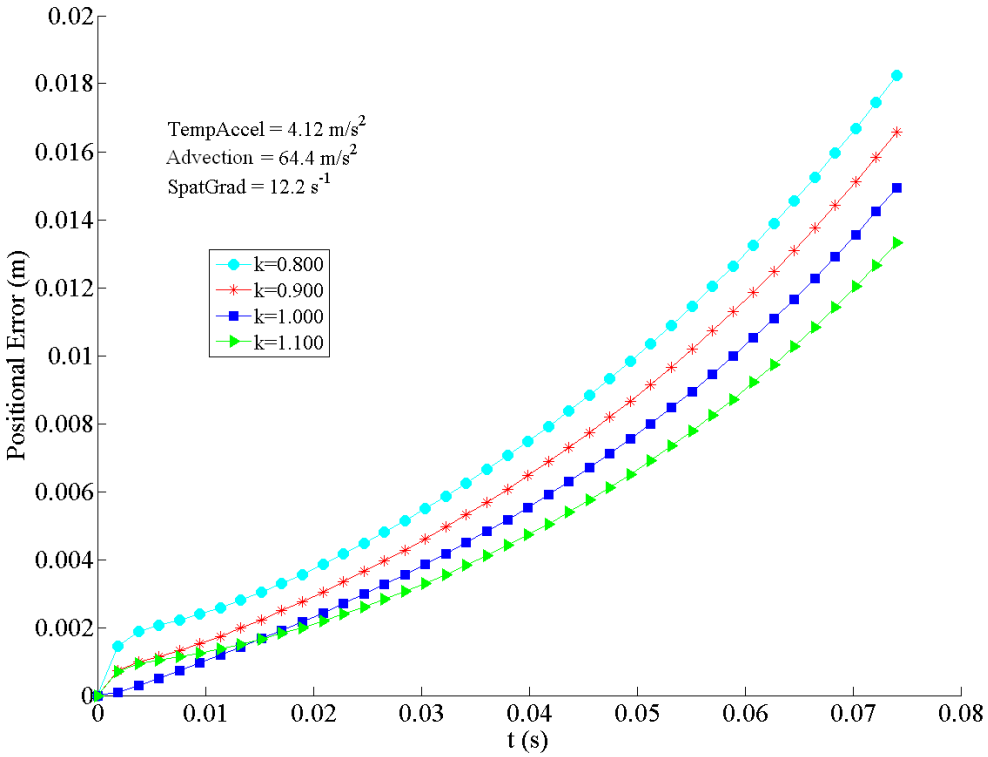

Figure 6.7: Influence of initial slip velocity in exponential behavior. Here, $a = \pi/2$, $d = \pi/4$, $t = 0$ through $50\tau_d \approx 0.075s$, and $k = 0.8$ through 1.1. Particle initial position is $(0.90, -0.53, 0.21)$.

The spacing between the plotted lines above does not remain constant as in the temporal case; rather it grows exponentially through time along with the error. This is not clear in the graph above, so the difference in error between the $k = 0.8$ case and the $k = 1$ case is plotted through time below.

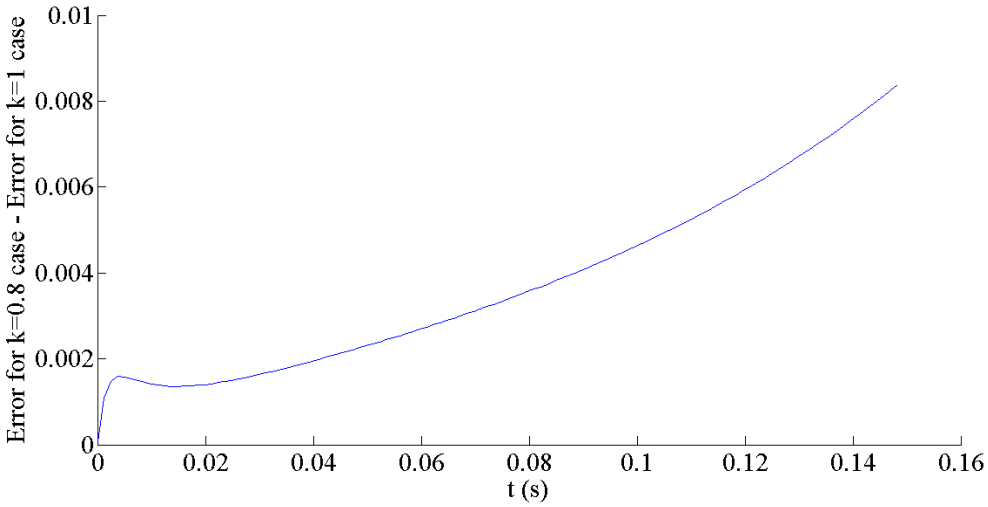

Figure 6.8: Growth in the slip velocity contribution to error. Here, $a = \pi/2$, $d = \pi/4$, $t = 0$ through $50\tau_d \approx 0.075s$, and $k = 0.8$ through 1.1. Particle initial position is $(0.90, -0.53, 0.21)$.

The exponential growth is a result of the presence of slip velocity terms in the coefficients of the governing exponentials $e^{\lambda t}$.

These simulations support the idea that the four factors observed to cause error in the one dimensional case, (exponent of the spatial gradient, advection, temporal acceleration, and initial slip velocity) translate well to the three dimensional case without introduction of any new factors. Depending on the flow field, errors may be treated as linear for a short time as long as the Stokes number and the spatial gradients are sufficiently small to control the exponential.

Chapter 7

Eulerian Viewpoint

In the Lagrangian perspective, the position discrepancy between equilibrium and full solution particles is allowed to change through time. The background flow field that an equilibrium or full solution particle sees as a result of this position discrepancy varies based on gradients in the background flow field and particle inertia. This perspective permits understanding of the spatial feedback loop and temporal contribution to error.

The Eulerian perspective, by the nature of the view, forces both equilibrium and full solution particles to reside in the same physical location. The inherent difference in background velocity due to separating particle positions cannot be easily incorporated into the Eulerian perspective. Rather, questions of whether or not the particle is in equilibrium and how it might diverge through time must be addressed from a single point. The two equations under consideration are,

$$\frac{d\boldsymbol{V}^f}{dt} = \frac{\boldsymbol{U} - \boldsymbol{V}^f}{\tau_p} + \boldsymbol{g} \qquad \boldsymbol{V}^{eq} = \boldsymbol{U} + \boldsymbol{g}\tau_p$$

with the d/dt operator referring to Lagrangian derivative following the particle. The governing equation for $\boldsymbol{V}^F - \boldsymbol{V}^{eq}$ at a point represents the Eulerian framework for the equilibrium problem. The first step in developing this expression is to rearrange the equilibrium equation, divide by τ_p, and adding it to the full equation. The result is

$$\frac{d\boldsymbol{V}^f}{dt} = \frac{\boldsymbol{V}^{eq} - \boldsymbol{V}^F}{\tau_p}. \tag{7.1}$$

This statement is only permitted because it is assumed that the equilibrium particle and the full particle are at the same position, otherwise two different $U(\boldsymbol{x}, t)$ terms would be present. In order to bring $V^F - V^{eq}$ into the first order derivative note that

$$\frac{d\boldsymbol{V}^{eq}}{dt} = \frac{d\boldsymbol{U}}{dt} \tag{7.2}$$

and subtract this from Eq. (7.1). Employing the notation $\aleph = \boldsymbol{V}^f - \boldsymbol{V}^{eq}$ produces

$$\frac{d\boldsymbol{\aleph}}{dt} = -\frac{\boldsymbol{\aleph}}{\tau_p} - \frac{d\boldsymbol{U}(\boldsymbol{x},t)}{dt} \tag{7.3}$$

An explicit expression for $\boldsymbol{\aleph}$ is developed by applying the integrating factor method to Eq. 7.3, followed by expanding the resulting expression by parts and neglecting terms proportional to $\tau_p^3(d^2\boldsymbol{U}/dt^2)$. The details of this are given thoroughly in Appendix D because the application of integration by parts to the analysis of integrodifferential equations is a useful technique that is not documented in most advanced calculus textbooks. The resulting expression is

$$\boxed{\boldsymbol{\aleph} = \boldsymbol{\aleph}^o e^{-t/\tau_p} - \tau_p \frac{d\boldsymbol{U}(\boldsymbol{x},t)}{dt} - \tau_p^2 \frac{d}{dt}\frac{d\boldsymbol{U}(\boldsymbol{x},t)}{dt} + \tau_p \frac{d\boldsymbol{U}^o}{dt} e^{-t/\tau_p}}. \tag{7.4}$$

This expression provides an idea of where in the flowfield the velocity error might be negligible. It says that if the it the equilibrium particle and the full solution particle remain at the same point, the error would consist of a constant velocity bias through the temporal and advective terms in $d\boldsymbol{U}/dt$ weighted by τ_p, as well as slip velocity effects that are expected to decay.

It is dangerous to evolve the equilibrium particle position error, $\int \boldsymbol{\aleph} dt$, through time using this equation because it can create a stiff problem. If this formulation is used, the timesteps must resolve exponential terms related to the flows spatial gradients that are not explicitly revealed by the Eulerian equation. Timesteps much smaller than τ_p must be employed, and even smaller timesteps may be necessary if the flowfield is varying quickly, which makes choosing the correct timestep size difficult. While Eulerian formulations can demonstrate important particle behavior, and may be used to solve for Lagrangian paths, they should not be used for the evolution of particle position for this reason. Instead, the general solution presented in Chapter 4 may be applied by determining $\mathbb{R}^4_{\text{lin}}$, and solving for the particle position and velocity explicitly. There are no timestep ambiguities, and all the behavior encapsulated by the heavy particle equation of motion is captured.

Chapter 8

Conclusions and Future Research

The answer to the question "is a particle in equilibrium" is more complicated than looking at the standard definitions of Stokes number. Using the heavy particle equation of motion, it has been shown that the primary parameter that governs the validity of the equilibrium assumption consists of the product of the eigenvalues of the flow velocity gradient tensor and the particle time constant, $\Lambda_{1-3}\tau_p$. This parameter is termed the heavy particle Stokes number. It is the most important source of error that a user must consider before applying the equilibrium approximation as it governs if errors will be linear or exponential.

Temporal acceleration, advection terms, and initial slip velocity all contribute secondary errors that must be considered as well. The significance of these errors, as well as their prediction, has been numerically demonstrated. These secondary errors arise through the coefficients of exponentials in the state space solution, which represent the eigenvectors of the state space matrix. In one dimension, the exact determination of these eigenvectors, along with the use of different expansions in $\sqrt{1+4\Lambda\tau_p}$, allowed for the complete understanding of these secondary errors. The lack of a concise explicit formula for the eigenvectors of the full 3D state space matrices prevents the accurate prediction of these errors in three dimensions. Nonetheless, the underlying mechanisms that govern the one-dimensional case translate well to the fully three dimensional case, as demonstrated in the benchmarking flowfield. Spatial and temporal variations in the flowfield must be addressed separately because they represent different mechanisms for how error accumulates through time. Temporal errors may be predicted exactly if spatial gradients are negligible, which decouples the governing equations of motion. In steady cases, such as the Stuart vortex, the heavy particle Stokes number governs the error associated with the equilibrium assumption.

As a result of this analysis, inherent disadvantages in using previously proposed Eulerian equations of motion for particle advection have arisen. Eulerian techniques provide no picture of how errors in their equation of motion grow through a particles trajectory, produce stiff computational problems, and still require the evolution of a particle position to determine regions of

preferential concentration precisely. The heavy particle Stokes number and the other discriminating parameters are simple to calculate, and thus may be used as a criterion for determining equilibrium, expediting Lagrangian calculations in CFD codes.

The full and equilibrium solutions for particle trajectories in a locally linear flow field have been obtained. These solutions may prove computationally beneficial, and are less complex than previously established methods that circumvent time marching algorithms. The equilibrium approximation may be employed in finding closure relations for the evolution of particle or droplet number density. These closure relations may be of use in developing multiple phase Lagrangian eddy simulation formulations. Particle equilibrium physics also finds use in quantifying if small particles are correctly acting as tracers in Particle Image Velocimetry. Incorporating the added mass term to the governing equation of motion would extend the applicability of this work to bubbly flows, and in certain conditions where the added mass term is negligible the analysis here may be used.

Appendix A

Trajectory Solutions

The full solution to the equation

$$\frac{d^2x_p}{dt^2} + \frac{1}{\tau_p}\frac{dx_p}{dt} - \frac{U_x^o}{\tau_p}x_p = \frac{U_t^o}{\tau_p}t = g + \frac{U^o}{\tau_p}. \tag{A.1}$$

is derived here using the state space system method. In matrix form, equation A.1 appears as

$$\begin{bmatrix} x_p' \\ V_p' \end{bmatrix} = \begin{bmatrix} 0 & 1 \\ \frac{U_x^o}{\tau_p} & -\frac{1}{\tau_p} \end{bmatrix} \begin{bmatrix} x_p \\ V_p \end{bmatrix} + \begin{bmatrix} 0 \\ \frac{U_t^o t}{\tau_p} + g - \frac{U_x^o X_o - U^o}{\tau_p} \end{bmatrix} = \boldsymbol{A} \begin{bmatrix} x_p \\ V_p \end{bmatrix} + \boldsymbol{b}. \tag{A.2}$$

The eigenvalues and eigenvectors of the state space matrix $\boldsymbol{A}$ are used to construct the solution to the system. For an n-equation system, the solution is of the form:

$$\boldsymbol{z(t)} = \sum_{i=1}^{n} C_i \boldsymbol{\eta_i} e^{\lambda_i t} + \boldsymbol{z(t)}_{particular} \tag{A.3}$$

as long as all the eigenvalues are distinct. Here $\boldsymbol{z(t)} = [X_p \quad V_p]$. The eigenvalues of $\boldsymbol{A}$ are

$$\lambda_1 = \frac{-1 + \sqrt{1 - 4U_x^o\tau_p}}{2\tau_p} \qquad \lambda_2 = \frac{-1 + \sqrt{1 + 4U_x^o\tau_p}}{2\tau_p}$$

The eigenvectors of $\boldsymbol{A}$ are[1]

$$\boldsymbol{\eta_1} = \begin{bmatrix} -\frac{-1+\sqrt{1+4U_x^o\tau_p}}{2U_x^o} \\ 1 \end{bmatrix} \qquad \boldsymbol{\eta_2} = \begin{bmatrix} -\frac{-1-\sqrt{1+4U_x^o\tau_p}}{2U_x^o} \\ 1 \end{bmatrix}$$

For the 1-d system we have $n = 2$ with a nonhomogeneous portion leading to a first order

[1] Obtained using Mathematica 5.1

polynomial in time as the particular solution.

$$\boldsymbol{z(t)} = C_1\boldsymbol{\eta_1}e^{\lambda_1 t} + C_2\boldsymbol{\eta_2}e^{\lambda_2 t} + t\boldsymbol{r} + \boldsymbol{s} \tag{A.4}$$

The particular solution is a solution of the system itself and is now solved for by plugging $\boldsymbol{z}_{part} = \boldsymbol{r}t + \boldsymbol{s}$ back into the original system (A.2).

$$\text{Using} \quad \boldsymbol{z_{part}} = t\begin{bmatrix} r_1 \\ r_2 \end{bmatrix} + \begin{bmatrix} s_1 \\ s_2 \end{bmatrix} \quad \text{and} \quad \boldsymbol{z'_{part}} = \begin{bmatrix} r_1 \\ r_2 \end{bmatrix}$$

$$\boldsymbol{r} = \begin{bmatrix} 0 & 1 \\ \frac{U_x^o}{\tau_p} & -\frac{1}{\tau_p} \end{bmatrix}(t\boldsymbol{r} + \boldsymbol{s}) + \begin{bmatrix} 0 \\ \frac{U_t^o t}{\tau_p} + g + \frac{U^o}{\tau_p} \end{bmatrix}$$

Equating powers of time (valid since there are no functions involved here) allows us to solve for the 4 unknowns.

$$\begin{bmatrix} 0 & 1 \\ \frac{U_x^o}{\tau_p} & -\frac{1}{\tau_p} \end{bmatrix} t\boldsymbol{r} = -\begin{bmatrix} 0 \\ \frac{U_t^o t}{\tau_p} \end{bmatrix} \qquad \boldsymbol{r} = \begin{bmatrix} 0 & 1 \\ \frac{U_x^o}{\tau_p} & -\frac{1}{\tau_p} \end{bmatrix}\boldsymbol{s} + \begin{bmatrix} 0 \\ g + \frac{U^o}{\tau_p} \end{bmatrix}$$

First for r $\quad \boxed{r_2 = 0} \quad \dfrac{U_x^o}{\tau_p} r_1 = -\dfrac{U_t^o}{\tau_p} \quad \boxed{r_1 = -\dfrac{U_t^o}{U_x^o}}$

Then for s $\quad \boxed{s_2 = -\dfrac{U_t^o}{U_x^o}} \quad 0 = \dfrac{U_x^o}{\tau_p}s_1 + \dfrac{U_t^o}{\tau_p U_x^o} + g + \dfrac{U^o}{\tau_p}$

$$\boxed{s_1 = -\frac{g\tau_p}{U_x^o} - \frac{U_t^o}{U_x^{o2}} - \frac{U^o}{U_x^o}}$$

This leaves the particular solution as

$$\boldsymbol{z}_{part} = \begin{bmatrix} -\frac{U_t^o}{U_x^o}t - \mathbb{Q} \\ -\frac{U_t^o}{U_x^o} \end{bmatrix} \qquad \text{with } \mathbb{Q} = \frac{U_t^o}{U_x^{o2}} + \frac{U_o}{U_x^o} + \frac{g\tau_p}{U_x^o} \tag{A.5}$$

The following equations are now used to solve for $C1$ and $C2$.

$$x_p(0) = 0 = C_1\left(-\frac{-1+\sqrt{1+4U_x^o\tau_p}}{2U_x^o}\right) + C_2\left(-\frac{-1-\sqrt{1+4U_x^o\tau_p}}{2U_x^o}\right) - \frac{U_t^o}{U_x^o}t - \mathbb{Q} \tag{A.6}$$

$$V_p(0) = V^o = C_1 + C_2 - \frac{U_t^o}{U_x^o} \tag{A.7}$$

The expressions for C_1 and C_2 that satisfy Eq. (A.6) are

$$C_1 = \frac{U_t^o}{2U_x^o} + \frac{V^o}{2} - \frac{U_o}{\sqrt{1+4U_x^o\tau_p}} - \frac{U_t^o}{2U_x^o\sqrt{1+4U_x^o\tau_p}} + \frac{V^o}{2\sqrt{1+4U_x^o\tau_p}} - \frac{g\tau_p}{\sqrt{1+4U_x^o\tau_p}} \tag{A.8}$$

$$C_2 = \frac{U_t^o}{2U_x^o} + \frac{V^o}{2} + \frac{U_o}{\sqrt{1+4U_x^o\tau_p}} + \frac{U_t^o}{2U_x^o\sqrt{1+4U_x^o\tau_p}} - \frac{V^o}{2\sqrt{1+4U_x^o\tau_p}} + \frac{g\tau_p}{\sqrt{1+4U_x^o\tau_p}} \tag{A.9}$$

The constants, eigenvalues, and eigenvectors are inserted back into Eq. (A.4), and after some simplification[1], the full solution is obtained.

$$\Delta x_p^F = -\mathbb{Q} - \frac{U_t}{U_x}t + \left[\frac{\mathbb{Q}}{2} + \frac{1}{\sqrt{1+4U_x\tau_p}}\left(\frac{\mathbb{Q}}{2} + \frac{U_t\tau_p}{Ux} + V_o\tau_p\right)\right] e^{\frac{-1+\sqrt{1+4U_x\tau_p}}{2\tau_p}t} \tag{A.10}$$

$$+ \left[\frac{\mathbb{Q}}{2} - \frac{1}{\sqrt{1+4U_x\tau_p}}\left(\frac{\mathbb{Q}}{2} + \frac{U_t\tau_p}{Ux} + V_o\tau_p\right)\right] e^{\frac{-1-\sqrt{1+4U_x\tau_p}}{2\tau_p}t} \tag{A.11}$$

$$\Delta V_p^F = e^{\frac{-1-\sqrt{1+4U_x^o\tau_p}}{2\tau_p}t}\left(\frac{U_t^o}{2U_x^o} + \frac{V^o}{2} - \frac{U_o}{\sqrt{1+4U_x^o\tau_p}} - \frac{U_t^o}{2U_x^o\sqrt{1+4U_x^o\tau_p}} + \frac{V^o}{2\sqrt{1+4U_x^o\tau_p}} - \frac{g\tau_p}{\sqrt{1+4U_x^o\tau_p}}\right) + \tag{A.12}$$

$$e^{\frac{-1+\sqrt{1+4U_x^o\tau_p}}{2\tau_p}t}\left(\frac{U_t^o}{2U_x^o} + \frac{V^o}{2} + \frac{U_o}{\sqrt{1+4U_x^o\tau_p}} + \frac{U_t^o}{2U_x^o\sqrt{1+4U_x^o\tau_p}} - \frac{V^o}{2\sqrt{1+4U_x^o\tau_p}} + \frac{g\tau_p}{\sqrt{1+4U_x^o\tau_p}}\right) - \frac{U_t^o}{U_x^o} \tag{A.13}$$

The algebra involved in explicitly determining the solution for three-dimensional flow fields is prohibitive. However, the method presented here is easily adapted to yield numerical solutions in three dimensions.

Appendix B

Temporal Limit Demonstration

The temporal limits of the 1D flow field solutions are not immediately obvious, so the following limit is demonstrated here.

$$\begin{aligned}\lim_{U_x^o \to 0} \Delta x_p^{eq} &= \lim_{U_x^o \to 0} \left[\left(\frac{g\tau_p}{U_x^o} + \frac{U_t^o}{U_x^{o2}} + \frac{U^o}{U_x^o} \right) e^{U_x^o t} - \frac{U_t^o}{U_x^o} t - \frac{g\tau_p}{U_x^o} - \frac{U_t^o}{U_x^{o2}} - \frac{U^o}{U_x^o} \right] \\ &= U^o t + g\tau_p t + U_t \frac{t^2}{2} \end{aligned} \tag{B.1}$$

The exponential is expanded as

$$e^{U_x^o t} = 1 + U_x^o t + \frac{U_x^{o2} t^2}{2} \cdots . \tag{B.2}$$

The expression is truncated at two terms because it is clear that if U_x^{o3} terms are left in they will disappear in the limit $U_x^o \to 0$ because there will be linear terms in U_x^o left over after being multiplied by $\left(\frac{g\tau_p}{U_x^o} + \frac{U_t^o}{U_x^{o2}} + \frac{U^o}{U_x^o} \right)$.

This leaves the limit as

$$\lim_{U_x^o \to 0} \left[\left(\frac{g\tau_p}{U_x^o} + \frac{U_t^o}{U_x^{o2}} + \frac{U^o}{U_x^o} \right) \left(1 + U_x^o t + \frac{U_x^{o2} t^2}{2} \right) - \frac{U_t^o}{U_x^o} t - \frac{g\tau_p}{U_x^o} - \frac{U_t^o}{U_x^{o2}} - \frac{U^o}{U_x^o} \right] \tag{B.3}$$

Expanding this out produces

$$\lim_{U_x \to 0} \left[g\tau_p t + \frac{U_t^o t}{U_x^o} + U_o t + \frac{g\tau_p U_x^o t^2}{2} + \frac{U_t^o t^2}{2} + \frac{U^o U_x t^2}{2} - \frac{U_t^o t}{U_x^o} \right] . \tag{B.4}$$

Evaluating the limit provides the final answer. Mathematica 5.1 and Matlab 7.4.0 were used to evaluate the limits of the full solution Δx_p^F and the approximate solutions Δx_p^{A1-3}.

Appendix C

The Relationship between λ and Λ

The characteristic polynomial of the full state space matrix (4.1) has seven terms with the following coefficients:

$$\begin{gathered}\lambda^6 : 1 \qquad \lambda^5 : \frac{3}{\tau_p} \qquad \lambda^4 : \frac{3}{\tau_p^2} - \frac{\mathrm{tr}(\nabla \boldsymbol{U})}{\tau_p} \qquad \lambda^3 : \frac{1}{\tau_p^3} - \frac{2\mathrm{tr}(\nabla \boldsymbol{U})}{\tau_p^2} \\ \lambda^2 : \frac{-\mathrm{tr}(\nabla \boldsymbol{U})}{\tau_p^3} + \frac{(\mathrm{tr}(\nabla \boldsymbol{U}))^2 - \mathrm{tr}((\nabla \boldsymbol{U})^2)}{2\tau_p^2} \\ \lambda^1 : \frac{(\mathrm{tr}(\nabla \boldsymbol{U}))^2 - \mathrm{tr}((\nabla \boldsymbol{U})^2)}{2\tau_p^3} \qquad \lambda^0 : \frac{-\det(\nabla \boldsymbol{U})}{\tau_p^3}.\end{gathered} \tag{C.1}$$

This characteristic polynomial may also be written in factored form as

$$(\lambda - a_1)(\lambda - a_2) \ldots (\lambda - a_6). \tag{C.2}$$

Substituting the supposed form

$$\lambda_{1-2} = \frac{-1 \pm \sqrt{1 + 4\Lambda_1 \tau_p}}{2\tau_p} \tag{C.3}$$

into $(\lambda - a_1)(\lambda - a_2)$ leads to the conclusion that

$$(\lambda - a_1)(\lambda - a_2) = \lambda^2 + \frac{\lambda}{\tau_p} - \frac{\Lambda_1}{\tau_p}. \tag{C.4}$$

The full characteristic polynomial is then

$$\left(\lambda^2 + \frac{\lambda}{\tau_p} - \frac{\Lambda_1}{\tau_p}\right)\left(\lambda^2 + \frac{\lambda}{\tau_p} - \frac{\Lambda_2}{\tau_p}\right)\left(\lambda^2 + \frac{\lambda}{\tau_p} - \frac{\Lambda_3}{\tau_p}\right). \tag{C.5}$$

Expanding this out, the coefficients of the powers of λ are

$$\begin{aligned}
&\lambda^6 : 1 \quad \lambda^5 : \frac{3}{\tau_p} \quad \lambda^4 : \frac{3}{\tau_p^2} - \frac{(\Lambda_1+\Lambda_2+\Lambda_3)}{\tau_p} \qquad \lambda^3 : \frac{1}{\tau_p^3} - 2\frac{(\Lambda_1+\Lambda_2+\Lambda_3)}{\tau_p^2} \\
&\lambda^2 : \frac{-(\Lambda_1+\Lambda_2+\Lambda_3)}{\tau_p^3} + \frac{\Lambda_1\Lambda_2+\Lambda_1\Lambda_3+\Lambda_2\Lambda_3}{2\tau_p^2} \\
&\lambda^1 : \frac{\Lambda_1\Lambda_2+\Lambda_1\Lambda_3+\Lambda_2\Lambda_3}{2\tau_p^3} \qquad \lambda^0 : \frac{-\Lambda_1\Lambda_2\Lambda_3}{\tau_p^3}.
\end{aligned} \tag{C.6}$$

The tensor invariants may be written in terms of the eigenvalues as (see, for instance [10])

$$I_{\nabla \boldsymbol{U}} = \mathrm{tr}(\nabla \boldsymbol{U}) = \Lambda_1 + \Lambda_2 + \Lambda_3 \tag{C.7}$$

$$\begin{aligned}
II_{\nabla \boldsymbol{U}} &= 1/2\left[(\mathrm{tr}(\nabla \boldsymbol{U}))^2 - \mathrm{tr}((\nabla \boldsymbol{U})^2)\right] \\
&= \Lambda_1\Lambda_2 + \Lambda_1\Lambda_3 + \Lambda_2\Lambda_3
\end{aligned} \tag{C.8}$$

$$III_{\nabla \boldsymbol{U}} = \det(\nabla \boldsymbol{U}) = \Lambda_1\Lambda_2\Lambda_3. \tag{C.9}$$

$$\begin{aligned}
I_{\nabla \boldsymbol{U}} &= \mathrm{tr}(\nabla \boldsymbol{U}) = \Lambda_1 + \Lambda_2 + \Lambda_3 \\
II_{\nabla \boldsymbol{U}} &= 1/2\left[(\mathrm{tr}(\nabla \boldsymbol{U}))^2 - \mathrm{tr}((\nabla \boldsymbol{U})^2)\right] \\
&= \Lambda_1\Lambda_2 + \Lambda_1\Lambda_3 + \Lambda_2\Lambda_3 \\
III_{\nabla \boldsymbol{U}} &= \det(\nabla \boldsymbol{U}) = \Lambda_1\Lambda_2\Lambda_3.
\end{aligned} \tag{C.10}$$

Substituting these relations into (C.1) shows that (C.1) and (C.6) are equivalent. This proves that (4.1) is the correct form for λ_{1-6} that expresses the eigenvalues of the full system in terms of the eigenvalues of the velocity gradient tensor. The same result holds in the two dimensional case, and follows a similar proof. The relationship can likely be proven for arbitrary dimension for a state space matrix in the form of (4.1), but is beyond the scope of this work.

Appendix D

Eulerian Error ODE Simplification

The Eulerian expression for the equilibrium error is

$$\frac{d\boldsymbol{\aleph}}{dt} = -\frac{\boldsymbol{\aleph}}{\tau_p} - \frac{d\boldsymbol{U}(\boldsymbol{x},t)}{dt},$$

which is equation 7.3. Using the integrating factor method, it is written as

$$\int_0^{t'} \left(\frac{d}{dt^*} e^{t^*/\tau_p} \boldsymbol{\aleph}(t^*) \right) dt^* = -\int_0^{t'} \left(e^{t^*/\tau_p} \frac{d\boldsymbol{U}(t^*)}{dt^*} dt^* \right) \tag{D.1}$$

$$\boldsymbol{\aleph}(t') - \boldsymbol{\aleph}^o e^{-t'/\tau_p} = -e^{-t'/\tau_p} \int_0^{t'} e^{t^*/\tau_p} \frac{d\boldsymbol{U}(t^*)}{dt^*} dt^* \tag{D.2}$$

Now allowing for $\frac{d\boldsymbol{Y}}{dt} = \boldsymbol{\aleph}$ and integrating gives

$$\int_0^{t} \left(\frac{d\boldsymbol{Y}(t')}{dt'} - \boldsymbol{\aleph}^o e^{-t/\tau_p} \right) dt' = -\int_0^{t} e^{-t'/\tau_p} \left(\int_0^{t'} e^{t^*/\tau_p} \frac{d\boldsymbol{U}(t^*)}{dt^*} dt^* \right) dt'$$

$$\boldsymbol{Y}(t) - \boldsymbol{Y}^o = \boldsymbol{\aleph}^o \tau_p \left(1 - e^{-t'/\tau_p} \right) - \int_0^{t} \left(e^{-t'/\tau_p} \int_0^{t'} \left(e^{t^*/\tau_p} \frac{d\boldsymbol{U}(t^*)}{dt^*} \right) dt^* \right) dt' \tag{D.3}$$

Integration by parts of the form $\int u dv = uv - \int v du$ is performed on the double integral.

$$u = \int_0^{t'} e^{t^*/\tau_p} \frac{d\boldsymbol{U}(t^*)}{dt^*} dt^* \qquad dv = e^{-t'/\tau_p} dt' \tag{D.4}$$

$$du = e^{t'/\tau_p} \frac{d\boldsymbol{U}}{dt'} dt' \qquad v = -\tau_p e^{-t'/\tau_p} \tag{D.5}$$

Note that the du comes from the fundamental theorem of calculus. Continuing,

$$\int_0^t \left(e^{-t'/\tau_p} \int_0^{t'} \left(e^{t^*/\tau_p} \frac{d\boldsymbol{U}(t^*)}{dt^*} \right) dt^* \right) dt' \tag{D.6}$$

$$= \int_0^t \tau_p \frac{d\boldsymbol{U}(t')}{dt'} dt' - \tau_p e^{-t'/\tau_p} \int_0^{t'} e^{t^*/\tau_p} \frac{d\boldsymbol{U}(t^*)}{dt^*} dt^* \tag{D.7}$$

The integral is factored out to express the equation as a single integral. This is most easily seen by replacing the t''s with t and the t^*'s with t in the second term.

$$\int_0^t \left(e^{-t'/\tau_p} \int_0^{t'} \left(e^{t^*/\tau_p} \frac{d\boldsymbol{U}(t^*)}{dt^*} \right) dt^* \right) dt' = \tag{D.8}$$

$$\tau_p \int_0^{t'} \frac{d\boldsymbol{U}(t^*)}{dt^*} \left(1 - e^{-t'/\tau_p + t^*/\tau_p} \right) dt^* = \tau_p \int_0^t \frac{d\boldsymbol{U}(t')}{dt'} \left(1 - e^{-t/\tau_p + t'/\tau_p} \right) dt' \tag{D.9}$$

Plugging this into D.3 gives

$$\boldsymbol{Y} - \boldsymbol{Y}^o = \boldsymbol{\aleph}^o \tau_p \left(1 - e^{-t/\tau_p} \right) - \tau_p \int_0^t \frac{d\boldsymbol{U}(t')}{dt'} dt' + \tau_p \int_0^t \frac{d\boldsymbol{U}(t')}{dt'} e^{-(t-t')/\tau_p} dt' \tag{D.10}$$

Integrating the second term by parts again

$$u = \frac{d\boldsymbol{U}(t')}{dt'} \qquad dv = e^{-(t-t')/\tau_p} dt' \tag{D.11}$$

$$du = \frac{d}{dt'} \frac{d\boldsymbol{U}(t')}{dt'} dt' \qquad v = -\tau_p e^{-(t-t')/\tau_p} \tag{D.12}$$

$$\int_0^t \frac{d\boldsymbol{U}}{dt} e^{-(t-t')/\tau_p} dt' = -\left[\frac{d\boldsymbol{U}}{dt} \tau_p e^{-(t-t')/\tau_p} \right]_{t'=0}^{t'=t} + \int \tau_p \frac{d}{dt} \frac{d\boldsymbol{U}}{dt} e^{-(t-t')/\tau_p} dt' \tag{D.13}$$

$$= -\tau_p \frac{d\boldsymbol{U}}{dt} + \tau_p \frac{d\boldsymbol{U}^o}{dt} e^{-t/\tau_p} + \int_0^t \tau_p \frac{d}{dt} \frac{d\boldsymbol{U}}{dt} e^{-(t-t')/\tau_p} dt' \tag{D.14}$$

Now reinserting the integral back into equation D.10 gives

$$\boldsymbol{Y}(t) - \boldsymbol{Y}(0) = \boldsymbol{\aleph}^o \tau_p \left(1 - e^{-t/\tau_p} \right) - \tau_p \int_0^t \frac{d\boldsymbol{U}}{dt} dt' \tag{D.15}$$

$$+ \tau_p^2 \left(-\frac{d\boldsymbol{U}}{dt} + \frac{d\boldsymbol{U}^o}{dt} e^{-t/\tau_p} + \int_0^t \frac{d}{dt} \frac{d\boldsymbol{U}}{dt} e^{-(t-t')/\tau_p} dt' \right) \tag{D.16}$$

The last term is proportional to $\tau_p^3 (d^2\boldsymbol{U}/dt^2)$ and is neglected. Differentiating provides Eq. (7.4), which is

$$\boldsymbol{\aleph} = \boldsymbol{\aleph}^o e^{-t/\tau_p} - \tau_p \frac{d\boldsymbol{U}(t)}{dt} - \tau_p^2 \frac{d}{dt} \frac{d\boldsymbol{U}}{dt} + \tau_p \frac{d\boldsymbol{U}^o}{dt} e^{-t/\tau_p}. \tag{D.17}$$

Bibliography

[1] A. Ahluwalia. Master's thesis, The Pennsylvania State University, 2002.

[2] Z. Dodin and T. Elperin. On the motion of small heavy particles in an unsteady flow. *Physics of Fluids*, 16(8):3231–3234, 2004.

[3] O.A. Druzhinin. On the two-way interaction in two-dimensional particle-laden flows: the accumulation of particles and flow modification. *Journal of Fluid Mechanics*, 297:49–76, 1995.

[4] C.R. Ethier and D.A. Steinman. Exact fully 3d navier-stokes solutions for benchmarking. *International Journal for Numerical Methods in Fluids*, 19:369–375, 1994.

[5] H. Faxen. Der widerstand gegen die bewegung einer starren kugel in einer zähen flüssigkeit, die zwischen zwei parallelen ebenen wänded eingeschlossen ist. *Annalen der Physik*, 4:89–119, 1922.

[6] S. Ferry, J. Balachandar. A fast eulerian method for disperse two-phase flow. *Int. J. Multiphase Flow*, 27:1199–1226, 2001.

[7] S. Ferry, J. Rani and S. Balachandar. A locally implicit improvement of the equilirbium eulerian method. *Int. J. Multiphase Flow*, 29:869–891, 2003.

[8] J. Eaton J. Fessler, J. Kulick. Preferential concentration of heavy particles in a turbulent channel flow. *Physics of Fluids*, 6(11):3742–3749, 1994.

[9] A. Goater. Dispersion of heavy particles in an isolated pancake-like vortex. Master's thesis, The University of British Columbia, 2003.

[10] Michael Itskov. *Tensor Algebra and Tensor Analysis for Engineers*. Springer, 2007.

[11] A.N. Kolmogorov. The local structure of turbulence in incompressible viscous fluid at very large reynolds numbers. *C.R. Acad. Sci. URSS*, 16:301, 1941.

[12] L. Liang and E.E. Michaelides. The magnitude of basset forces in unstead multiphase flow computations. *Jour. of Fluids Eng.*, 1992.

[13] M. Maxey and J. Riley. Equation of motion for a small rigid sphere in a nonuniform flow. *Physics of Fluids*, 26(4), 1983.

[14] M.R. Maxey. The gravitational settling of aerosol particles in homogeneous turbulence and random flow fields. *Journal of Fluid Mechanics*, 174:441–465, 1987.

[15] R. Mei and R.J. Adrian. Flow past a sphere with an oscillationn in the free-stream and unsteady drag at finite reynolds number. *Journal of Fluid Mechanics*, 237:323–341, 1992.

[16] E.E. Michaelides. Review - the transient equation of motion for particles, bubbles, and droplets. *Jour. of Fluids Eng.*, 119:233–247, 1997.

[17] E. Mograbi and E. Bar-Ziv. Local effects of st o(1) on small particle motion in a linear flow field. *Physics of Fluids*, 17, 2005.

[18] S.A. Poison. Memoire sur les mouvements simulatanes d' un pendule et de l' air environnant. *Mem. de l' Academie des Sciences, Paris*, 9:521–523, 1831.

[19] L. Reade, W. Collins. Effect of preferential concentration on turbulent collision rates. *Physics of Fluids*, 12(10):2530–2540, 2000.

[20] P.J. Saffman. The lift on a small sphere in a slow shear flow. *Journal of Fluid Mechanics*, 22:385, 1965.

[21] I. Silverman and W.A. Sirignano. Multidroplet interaction effects in dense sprays. *Inter. Journ. of Multiphase Flows*, 20:99–116, 1994.

[22] J.T. Stuart. On finite amplitude oscillations in laminar mixing layers. *Journal of Fluid Mechanics*, 29:417–440, 1967.

[23] F. Takemura and J. Magnaudet. The history force on a rapidly shrinking bubble rising at finite reynolds number. *Physics of Fluids*, 16(9):3247–3255, 2004.

[24] H. Tennekes and J.L. Lumley. *A First Course in Turbulence*. MIT Press, 1972.

[25] T.R. Wang, S. Troutt and C.T. Crowe. Bubble dispersion in vortical flows. *Gas-Liquid Flows*, 165:171–176, 1993.